Late Permian to early Middle Triassic palaeoenvironmental reconstructions of the High Atlas, Morocco: Geodynamic and climate implications in the intertropical western Peri-Tethyan domain

Naima Benaouiss, Abdelilah Tourani, Sylvie Bourquin, Nour-Eddine Eddine Jalil

Late Permian to early Middle Triassic palaeoenvironmental reconstructions of the High Atlas, Morocco: Geodynamic and climate implications in the intertropical western Peri-Tethyan domain

Naima Benaouiss, Abdelilah Tourani, Sylvie Bourquin, Nour-Eddine Jalil

PII: S0031-0182(23)00427-3

DOI: https://doi.org/10.1016/j.palaeo.2023.111809

Reference: PALAEO 111809

To appear in: *Palaeogeography, Palaeoclimatology, Palaeoecology*

Received date: 9 March 2023

Revised date: 31 July 2023

Accepted date: 7 September 2023

Please cite this article as: N. Benaouiss, A. Tourani, S. Bourquin, et al., Late Permian to early Middle Triassic palaeoenvironmental reconstructions of the High Atlas, Morocco: Geodynamic and climate implications in the intertropical western Peri-Tethyan domain, *Palaeogeography, Palaeoclimatology, Palaeoecology* (2023), https://doi.org/10.1016/j.palaeo.2023.111809

Late Permian to early Middle Triassic palaeoenvironmental reconstructions of the High Atlas, Morocco: geodynamic and climate implications in the intertropical western Peri-Tethyan domain

Naima Benaouiss[1*], Abdelilah Tourani[1], Sylvie Bourquin[2], Nour-Eddine Jalil[3]

[1]Département de Géologie, Faculté des Sciences Semlalia, Université Cadi Ayyad, Boulevard Prince Moulay Abdellah, BP: 2390, Marrakech, Maroc, benaouiss@uca.ma and tourani@uca.ma

[2]Univ Rennes, CNRS, Géosciences Rennes – UMR CNRS 6118, F-35000, Rennes, France, sylvie.bourquin@univ-rennes1.fr

[3]Centre de Recherche en Paléontologie – Paris CR2P - UMR 7207 MNHN, case postale 48, 57 rue Cuvier, F-75231 Paris cedex 05 (France), nour-eddine.jalil@mnhn.fr

[*]Corresponding author. E-mail address: benaouiss@uca.ma (N. Benaouiss).

Abstract

This study characterizes the depositional environment and climate evolution from the late Permian to the early Middle Triassic, based on detailed sedimentological and palaeosol analysis. Sequence stratigraphy and palaeoenvironmental reconstructions were used to define the Permian-Triassic (P-T) evolution of the High Atlas basins as well as to make a comparison with European basins.

The late Permian in Morocco is dominated by distal fluvial fan environment, under arid to semi-arid paleoclimate conditions. Above the P-T unconformity (BS1), the Lower Triassic deposits, record a similar climate evolution from arid to subhumid conditions. In the Argana Basin, the Early Triassic starts by an aeolian deflation lag, followed by stacked debris flow lobes and sheetflood ephemeral alluvial fan deposits, showing immature to locally mature calcretes. The Marrakech High Atlas basins are further characterized by well-developed aeolian dunes in alluvial fan environment. These arid environments evolve through time from proximal to distal deposits, as a retrogradational trend, until well-developed floodplain or lacustrine deposits under semi-arid to subhumid climate (maximum flooding surface, MFS). From MFS, the evolution from distal to proximal environments, testified the progradational trend which is capped by a newly defined angular unconformity (BS2). Above this tectonically induced BS2, the sedimentary section, dated as Anisian is characterized by palaeoenvironments that include meandering river fluvial packages deposited in a semi-arid floodplain.

Basin configuration, border fault direction, palaeoenvironments and palaeocurrents recorded in the Argana Basin confirm an independent system, separate from the Marrakech High Atlas (MHA) area during the Triassic. Above BS1, remnant topographies resulted in

discrete catchment and discrete drainage systems are evidenced by palaeocurrent and palaeowind measurements controlled by border faults. Palaeoenvironment reconstructions show that the MHA was made up of numerous independent basins during the Early Triassic and the remnant topographies are progressively infilled until BS2. After the BS2, the palaeo-drainage became axial and basins were probably connected in the MHA. Above the P-T unconformity, a common climate evolution is observed in Morocco during the Lower Triassic until BS2, which could correspond to the European Hardegsen unconformity. The sedimentation record shows a similar change in climate and geodynamics to that recorded from both Europe and Morocco.

Keywords

Permian-Triassic unconformity; Palaeosol analysis; Alluvial fan; Aeolian and lacustrine; Marrakech High Atlas; Argana.

1. Introduction

The Permian-Triassic (P-T) boundary is an important time interval that has been intensely studied across the world to document changes in climatic, biotic and environmental conditions, especially on terrestrial successions. This transition contains the P-T mass extinction that was the most devastating biocrisis of life on Earth, both in terrestrial and marine ecosystems (Burgess et al., 2014; Erwin, 1994; Meijer, 2007). Distinct perturbations are related to a major climate change as, (1) prominent negative carbon-isotope excursion (Baud et al., 1996; Galfetti et al., 2007; Payne et al., 2004; Shen et al., 2023), (2) terrestrial spore-pollen assemblages, (3) ammonoid distribution patterns and (4) high diversity in plant ecosystems (Galfetti et al., 2007; Rees, 2002).

At the scale of the western European peri-Tethyan basins, the late Permian is characterized by warm and semi-arid climatic conditions (Schneider et al., 2006) and an unconformity is observed almost everywhere between the Permian and Triassic, except in the central part of the Germanic Basin (e.g., Bourquin et al., 2011). During the Induan, all intra-belt basins were under erosion and sediment was only preserved in the northern domain under similar climatic conditions as during the latest Permian (the central part of the Germanic Basin; e.g., Ravidà et al., 2022; Schneider et al., 2020). Mesozoic sedimentation began in the early Olenekian; with ephemeral fluvial systems indicating arid climatic conditions during this period (e.g., Bourquin et al., 2009, 2007). At the top of the Early Triassic, another tectonically induced, often angular, unconformity is observed: the Hardegsen unconformity, which is dated as intra-Spathian (Geluk and Röhling, 1997; Szurlies, 2007, 2004) and is especially found in northern European basins. This tectonic activity created new source areas and a new fluvial style, with marine influences at the distal part of the systems (Bourquin et

al., 2011). Both at the end of the Olenekian (Spathian) and during the Anisian, the presence of palaeosols, micro- and macrofloras indicate less arid conditions throughout this domain.

Although it is considered that the Triassic red-beds record the early stages of the rifting, preceding the opening of the Central Atlantic Ocean (Domènech et al., 2015; El Arabi et al., 2006; Le Roy and Piqué, 2001; Olsen et al., 2003), the timing and basin evolution (independent or connected basins) is still unknown. Our aim is to define more precisely the evolution of the High Atlas basins from the P-T unconformity to the early Middle Triassic. Within the High Atlas, the Permian and Triassic sedimentation settled in a terrestrial environment and formed thick red siliciclastic series. The present study, based on a detailed sedimentological and palaeosol analysis, defines for the first time the palaeoenvironment and climate evolution from the late Permian to early Middle Triassic in the Marrakech High Atlas (MHA) and Western High Atlas (WHA) basins (Fig.1A). Based on the sequence stratigraphy, the study also attempts to make a regional correlation between the MHA and Argana basins, in order to understand the geodynamic evolution of the High Atlas basins. Moreover, a comparison between these Moroccan basins and European basins allows discussing the climate and geodynamic evolution of the western peri-Tethyan domain during the end of the Palaeozoic to the beginning of the Mesozoic.

2. Geological setting

In Morocco, P-T basins were developed in a transtensional rift system, before the opening of the Central Atlantic Ocean (Beauchamp, 1988; Beauchamp et al., 1999; Domènech et al., 2015; Frizon de Lamotte et al., 2009; Laville et al., 2004; Laville and Piqué, 1991; Manspeizer, 1988; Manspeizer et al., 1978; Missenard et al., 2007; Stets and Wurster, 1982). The Permian and Triassic basins overlie the deformed Variscan basement, represented by Precambrian volcanic rock, Cambrian series granitoids and metamorphic rocks, and

Carboniferous mudstones. This basement is affected by NNE-SSW to NW-SE and E-W folds (Cornée, 1989; Jenny, 1983; Laville, 1980; Ouanaimi and Petit, 1992). Triassic sedimentation was controlled by both dip-slip and strike-slip synsedimentary faulting, reactivated from Hercynian faults (Baudon et al., 2009; El Arabi, 1988; El Arabi et al., 2003; Laville and Petit, 1984; Laville and Piqué, 1991).

During the Permian to Early Jurassic, the MHA and Argana basins (Fig. 1B) were separated by the "Massif Ancien" High (Domènech et al., 2015; Fabuel-Perez et al., 2009; Ouanaimi, 1989). The Argana Basin, oriented NNE-SSW, was controlled by normal NE-SW system faults and E-W transform faults (Baudon et al., 2009; Ellouz et al., 2003; Medina, 1994; Oliva-Urcia et al., 2016; Proust et al., 1977). Extrusive basaltic volcanism, associated with the Central Atlantic Magmatic Province (CAMP) (Fig. 1C), is associated with the border fault zones. Dated as Early Jurassic, this basalt represents an important stratigraphic marker across Morocco (Aït Chayeb et al., 1998; Bertrand et al., 1982; Blackburn et al., 2013; De Pachtère, 1983; Marzoli et al., 2004)

The Permian-Lower Triassic red-bed series of the studied interval, in the Argana Basin, are defined as (Fig. 1C): (1) the Ikakern Formation (Fm) is divided into the t1 and t2 units, (2) the Timezgadiwine Fm is divided into the t3, t4 and t5 units (Tixeront, 1974, 1973). The t2 Unit (Fig. 1C) is dated from vertebrate remains as late Permian (Lopingian) (Jalil and Dutuit, 1996; Jalil and Janvier, 2005). It is characterized by mainly very fine sandstones, mudstones, and interbedded subordinate conglomerates to pebbly coarse sandstones, attributed to a meandering fluvial environment (Tourani et al., 2000). Above the P-T angular unconformity (Baudon et al., 2009; Duffaud et al., 1966; Tixeront, 1973), the first Mesozoic deposits (t3 Unit, Fig. 1C), tentatively dated from tetrapod footprints as Early Triassic (Olenekian) (Tourani et al., 2010), are characterized by interbedded conglomerates and cobbly coarse- to

fine-grained sandstones attributed to proximal braided rivers (Tourani et al., 2000). The overlain t4 Unit (Fig. 1C) is also dated Olenekian at its base from tetrapod footprints (Klein et al., 2010). Above this level, the t4 Unit (Fig. 1C) is dated Anisian from charophytes and ostracods (Medina et al., 2001), vertebrate remains (Jalil et al., 2009) and tetrapod footprints (Klein et al., 2011). This unit is composed of siltstones with interbedded conglomerates and sandstones, interpreted as meandering rivers (Tourani et al., 2000).

Within the MHA basins, Biron (1982) established the stratigraphic nomenclature of the Permian and Triassic units (Fig. 1C). The lower and upper parts of the Permian successions are respectively composed of the Anrar Conglomerate Fm. or F1 Unit and the Cham-el-Houa Siltstone Fm or F2 Unit. Using radiometric dating, Van Houten (1977) attributes a Cisularian age, i.e., early Permian, to the F1 Unit (Fig. 1C), while Biron (1982) considers the F1 and F2 units as early Permian. However, more recently, the F1 Unit is dated as late Permian (Lopingian), using zircon geochronology (Perez et al., 2019). The F2 Unit (Fig. 1C), attributed to a braid-plain that evolved vertically to anastomosing river deposits (Benaouiss and Courel, 1993), is considered as late Permian by correlation with the t2 Unit of the Argana Basin (El Arabi et al., 2006). Above the P-T unconformity, the Mesozoic Timalizène Conglomerate Fm or F3 Unit (Fig. 1C), is considered as fluvial deposits (Biron, 1982). The F3 Unit is overlain by the Ramuntcho Siltstone Fm (Mattis, 1977) or the Anouffig Siltstone Fm (F4 Unit, Biron, 1982). There is controversy in the literature concerning the interpretation of the depositional environment for this unit. Different environments suggested are (a) river / floodplain (Mattis, 1977) and (b) tidal-flat environment (Petit and Beauchamp, 1986) with burrows and rare molds of littoral marine bivalves (Beauchamp and Petit, 1983; Biron, 1982). The F4 Unit (Fig. 1C) is dated by palynomorphs, as Middle Triassic (Anisian) (El Arabi et al., 2006).

3. Methodology

Three sections were studied in detail, from southwest to northeast, one in the Argana Basin (Irerhi section) and two within the Marrakech High Atlas (Tanoumri and Aït Tamlil sections) (Fig. 1B). To interpret the depositional environment, a detailed sedimentological study was performed including (1) facies, (2) facies association, (3) palaeocurrent, (4) palaeosol and (5) burrow analyses. The architectural elements and their large-scale bed relationships, both vertically and horizontally, were defined. Subsequently the architectural elements according to facies associations, palaeocurrent measurements and identification of unconformities were used to characterize and reconstruct the depositional environment evolution for each section. This was used to define stratigraphic cycles based on the sequence stratigraphy, i.e. progradation and retrogradation, which reflect control by accommodation, climate combined with variations in sediment supply (for continental deposits, e.g., Bourquin et al., 2009, 1998; Currie, 1997; Olsen, 1995). The climatic evolution was based on sedimentological and palaeosol criteria. Pedogenic calcretes and soil types were defined from Esteban and Klappa (1983), Mack et al. (1993), Retallack (1988), Sheldon and Tabor (2009), Tabor and Montañez (2004), and Wright and Tucker (1991). Alonso-Zarza (2003) reviewed and specified the palaeoenvironmental significance of these soils. The palaeosol classification used is based on those of Mack et al., (1993) and Tabor and Montañez (2004). The stratigraphic cycles combined with climate evolution made it possible to propose correlations and to discuss the importance of the unconformities at the Morocco High Atlas scale. All these data were compiled into palaeoenvironmental reconstructions, including palaeocurrent and palaeowind directions at the scale of the MHA that allowed discussion of the evolution of the depositional environment, through time and space, in relation to climate. By suggesting a correlation with European basins, it then becomes possible to discuss tectonic and climate controls at the scale of the western peri-Tethyan domain.

4. Sedimentological analysis and depositional environments

Thirty-one facies were identified in the sedimentological study of the High Atlas basins: eight conglomerate, thirteen sandstone, four mudstone, four carbonate, and two heterolithic facies (Table 1). The 16 facies associations, including bioturbation and palaeosol descriptions, were used here to define 11 depositional environments ranging from alluvial to lake or aeolian (Table 3). Results are presented for the three sections: the Irerhi section (30° 49' 55.35"N, 9° 5' 35.87"W) in the Argana Basin and the Tanoumri (31° 21' 50.04"N, 7° 44' 13.02"W) and Aït Tamlil (31° 28' 23.04"N, 6° 53' 52.38"W) sections in the MJA basins (Fig. 1B).

4.1. Facies associations and depositional environments of the Argana Basin

In the Argana Valley, the Upper Permian t2 Unit, the regional unconformity between the t2 and t3 units, and the Lower Triassic t3 and t4 units are well exposed in the Irerhi area (Figs. 1, 2, 3, and 4A).

4.1.1. Late Permian depositional environments

Only the unit immediately below the top P-T unconformity was examined in this study. The upper part of the t2 Unit (Fig. 2) is mainly composed of the fine-grained sediments (Fsm facies, Table 1) that are modified by soils (Pv, Pc, Table 2) and interbedded with sandy facies. These sandy beds, up to 10-cm thick and 50-m long, are composed of horizontal laminations and current ripples (respectively Sh and Sr facies, Table 1). The facies association (Sh, Sr, Table 3) characterizes sandstone bodies with a flat base and irregular top. They are interpreted as terminal splays bodies, i.e., deposited by frontal sheetflood events in the fluvial fan environment (Fisher et al., 2008, 2007; Nichols and Fisher, 2007). This facies association is typical of distal fluvial fans in arid to semi-arid alluvial plains (named FF, Table 3). The palaeocurrent measurements, from parting lineation structure, reveal locally a NW-SE current direction, and a NW direction from current ripple laminations.

4.1.2. Lower Triassic depositional environments

The t3 Unit is approximately 11-m thick, and rests in angular unconformity on the t2 Unit (Figs. 2, 3A, 3B). The first t3 Unit deposits are composed of quartzite ventifacts characterized by very coarse pebbles to fine cobbles (DL facies, Table 1). These are aligned horizontally just above the Permian unconformity and form a bed of ventifacts up to 18 cm thick (Figs. 2, 4B and K). This facies association is characterized by an aeolian deflation lag surface and represents desert pavement, named RE facies association (Table 3).

Above this regional deflation surface (Fig. 2) recognized in several localities in the Argana Basin, the facies association (up to 1.8 m thick) is composed of a stacked bed up to 1.5m of sandstones and conglomerates (the Sm and Gmm facies, respectively, Table 1) that may contain ventifacts in the first 80 cm of the succession. This facies association is interpreted as debris flow lobes and characterizes the proximal alluvial fan deposits (AFp facies association, Table 3, and Fig. 4B). These deposits are overlain by three facies associations: one composed of conglomerates (G/S, Ga, Sm facies, Table 1), one composed mainly of sandstones (Sm, Sp, Sh, Sr facies, Table 1) and a last one composed of siltstones (Fm, Fsm facies, Table 1) beds (Fig. 2). The conglomerate facies association is mainly composed of gravely to sandy lobes, 40 to 80-cm thick and with a lateral extent of more than 1 km, stacked into units that are 1.25 to 2.5-m thick. These deposits characterize sheetflood from med-alluvial fan environments with an ephemeral stream named AFm1, (Table 3, and Fig. 4C) and are associated with calcisols, classified as Pc-IV or Pc-V based on the scheme of Machette (1985), which attests to an arid climate condition (Table 2). The Ga facies, interpreted as antidune backsets (Table 1) and recorded an up-fan palaeocurrent towards the north (Fig. 2), suggesting deposition from an alluvial fan flowing southward. The sandy facies association, composed beds that are between 70 cm and 1 m thick and extending up to 50 m with a generally flat base, show pedogenic features of Pc soil (Table 2) with horizontal

rhizoliths and locally covered by a carbonate horizon, i.e. stage V in Machette (1985). This facies association represents sandflat beds of a distal alluvial fan environment, named AFd (Table 3). Palaeocurrents, measured from the Sp facies, are oriented to the NW direction (Fig. 2). At the top of the t3 Unit, the AFd is interbedded with floodplain deposits (FP facies association, Table 3), displaying only the Fm facies (Fig. 2), where poorly drained soils (Pg, Table 2) attest to a subhumid climate. The upper part of the t3 Unit is characterized by conglomerates (Gt and Gp facies, Table 1), with 45 cm-thick sets of cross bedding and up to 1.80 m-thick cosets (Fig. 2). The base is generally flat to slightly erosive and the top is irregular and the palaeocurrent measurements indicate a flow direction mainly towards the NE and NW (Fig. 2). These stacked facies are typical of widespread braided streams and is named the RB facies association (Table 3, and Fig. 4A).

It is possible to observe a clear evolution from an arid climate to subhumid conditions within this section, with a less arid condition around 6m on the measured section (Fig. 2) from the base; this allows the t3 Unit to be divided into two subunits. The t3a Subunit (Fig. 2) is characterized by alluvial fan deposits (AFp, AFm1 and AFd) within an arid alluvial plain with ventifacts (Fig. 4K) at the base (DL, Table 1), often reworked by mass flow (Gmm, Table 1 and Fig. 4B) and interpreted as desert pavement (RE, Table 3). The overlying t3b Subunit (Fig. 2) displays more a humid condition, a semi-arid climate, with floodplain (FP) and distal alluvial fan deposits (AFd) that evolve vertically to a braided river (RB).

Conformable on the t3 Unit, the t4 Unit can be also subdivided into two subunits, named t4a and t4b respectively (Fig. 2), separated by an angular unconformity that is well-marked by a white soil surface (Pg soil, Table 2, Figs. 3C and 4D). According to the ages on each side of the discordance (Fig. 2), the base of the t4a Subunit is Lower Triassic (Klein et al., 2010), its upper part is Middle Triassic (Medina et al., 2001) and the t4b Subunit is Middle Triassic at

its base (Jalil et al., 2009) and at 45 m above the angular unconformity (Klein et al., 2011). The discordance is assigned to the early-Middle Triassic transition. The t4a Subunit has silty sandstone at the base (Sr, Sh facies, Table 1), with sets up to 1.5 m thick and extending more than 800 m, characterized by slightly inclined beds (3°). These facies are overlain by 3.5 m of siltstones to fine sandstones (Sr, Sl facies, Table 1) interbedded with fine-grained sediments (Fm facies, Table 1). This subunit displays root traces and mottling, characteristic of poorly drained soils (Pg, Table 2 and Fig. 4D) typical of humid conditions. This facies association is interpreted to sandy sheetflood deposits and corresponds to a distal alluvial fan in a subhumid context (named AFd, Table 3 and Fig. 4E).

4.1.3. Basal part of Middle Triassic depositional environments

The t4b Subunit rests unconformably on the t4a Subunit (Figs. 3C and 4D). This 6 m thick interval (Fig. 2) is mainly composed of a silty claystone facies (Fsm, Table 1) with calcic vertisols (Pv soil, Table 2) and rare interbedded micro-conglomerate facies (Gmi, Table 1). The lenticular shape of Gmi facies, up to 15 cm thick and 30 m length, is comprised of reworked carbonates from the floodplain, during the degradation-aggradation phases (Marriott and Wright, 2006; Smith and Kitching, 1997). The Pv soil characterizes a contrasting dry/wet climate favouring the degradation-aggradation of the floodplain, recorded by the Gmi facies. This facies association is typical of a floodplain in a semi-arid climate condition (FP facies association, Table 3).

4.2. Facies associations and depositional environments of the Marrakech High Atlas basins

In the MHA basins (Fig. 1B) the Lower Triassic succession (F3 Unit) rests unconformably on the Permian strata (F2 Unit; Figs. 5A, 5B, 5D to 5F), on either Palaeozoic or Precambrian crystalline rocks. Two sections have been described in the MHA basins

(Fig. 1B): one in the western part, i.e., Tanoumri section, and the other in the eastern part, i.e., Aït Tamlil section.

4.2.1. Tanoumri section

The Tanoumri section is located in the western part of the MHA, to the south of Marrakech (Figs. 1B, 5A, 5B, and 6).

Upper Permian depositional environments

The uppermost part of the F2 Unit (Fig. 6), mainly characterized by fine-grained facies (Fsm, Table 1), up to 4 m thick, is modified by cracking horizon, wedge-shaped peds, slickensides horizon, and centimetre-sized carbonate nodules typical of calcic vertisols (Pv, Table 2). The wedge-shaped slickensides and up to 1 cm carbonate nodules in mudstone host rock, are interpreted as calcisols (Pc, Table 2). Mainly mottled Fsm facies with root traces characterize hydromorphic soils (Pg, Table 2). Thin sandy bodies are interbedded up to 35 cm thick and extend up to 70 m, mainly composed of Sp, Sr and more rarely of Sh and Sm (Table 1 and Fig. 4F). These deposits characterize terminal splays with palaeocurrents oriented in a NNW to NNE direction. At the top of the F2 Unit, laminated carbonate facies are interbedded with brecciated claystone (C/C facies; Table 1; Figs. 4G, H, and I) up to 30 cm thick. This facies association is typical of a distal fluvial fan (FF) that evolves locally to a pond or shallow lake (PA; Table 3; Fig.4G, 4H, and 4I) with a slightly saline mudflat containing tabular-prismatic gypsum crystals (Benison and Goldstein, 2001; Mees et al., 2012). As attested by the soil developments, the climate was arid to semi-arid under contrasting dry/wet seasons, with dominant wet seasons towards the top.

Lower Triassic depositional environments

In the Tanoumri section, the F3 Unit (Figs. 5 A, 5B, and 6) rests on the F2 Unit by angular unconformity (Fig. 4F), and reveals conglomerates (DL, Gmm, GP, Gh, Gm, Ga, G/S, Table 1), sandstones (St, Sp, Sh, Shg, Sl, Sm, Sq, Ad, Ah, Ar, Table 1), carbonates (C/S, Cpa, Cpe, Table 1) and very rare fine-grained materials (Fsm, Table 1).

This Triassic succession starts with monogenic conglomerates (quartzite pebbles), horizontally aligned (Figs. 4J, and 6), forming a pebble- and cobble-sized ventifacts horizon (DL facies, Table 1). This horizon of wind-polished stones represents a deflation lag surface of desert pavement (RE, Table 3; Fig. 4J, and 4K). The ventifacts can be reworked by the superimposed Gmm facies in a silty matrix-supported (Table 1 and Figs. 4J, 4M). These deposits are overlain by Gmm, G/S, Ga, Gm, and Ar facies. The Gmm facies (Table 1 and Figs. 4J, 4M) is characterized by ventifacts reworked by mass flow and forming levees or lobes in proximal alluvial fan (AFp, Table 3). The Gm facies is composed of pebbles and cobbles clast- to matrix-supported with erosive base, interpreted as lag or gully-fill deposits (Table 1 and Figs. 4L, 4M). The planar gravelly-sandy couplets, showing imbricated gravel fabric and structureless to laminated sandstone (G/S, Table 1 and Fig. 4L) and sandy-pebbles with simple planar cross bedding, under upper-flow-regime sheetflood, that forms backset wedges or antidunes (Ga, Table 1 and Figs. 4L, 4M).. The sheetflood sequences can be capped by inversely graded ripples cross-laminated sandstone, these wind ripples are interpreted as simple aeolian drift (Ar facies, Table 1 and Figs. 4L, 4M). All these previous facies represent mid-alluvial fan deposits dominated by ephemeral sheetflood events (AFm1, Table 3). The palaeocurrent measurements from imbrications (noted "imbr" Fig. 6) are characterized by radial dispersion in time and space and display an angle of dispersion of 80° (from N30 to N310). The backsets give an upfan direction towards N100 to N190 (Ga, Fig. 6), which implies a flow of alluvial fans towards N280 to N10. The aeolian drift facies (Ar, Fig. 6) give an upfan direction towards N170 to N200. Consequently, the synthesized currents

of the alluvial fans were towards a NNE to W direction (N30 to N280), with a dispersion angle of 110°. Above AFm1, a stream flow and then aeolian dunes and a sand sheet (Ad and Ah facies, Table 1) are observed. Gravely or sandy facies (St, Sp, Sh, Sr and Sm facies, Table 1) with a thin coarse base (Gp, Gh facies, Table 1) up to 12.5 m-thick, characterizes more distal mid-alluvial fan deposits, named AFm2 in this work (Table 3). The stream flows are mainly composed of 2D/3D bedforms and gravely or sandy bars. Carbonate accumulations are common within AFm2, in mainly sandstone host rocks with circular to ovoid carbonate nodules shape and in the conglomerate host rocks (6 to 7.5 m and 11.2 to 11.5 m levels, Fig. 6) with calcite under-coated gravel, both characterizing immature calcisols (Pc palaeosol, stage II of Machette (1985), Table 2). The 18 m level of Figure 6 shows the second horizon of ventifacts composed of quartz pebbles (DL, Table 1), and it represents a well-extended deflation lag surface or desert pavement named erg deposits in this section (RE). Well sorted sandstones and solitary large-scale planar cross-bedded bedform that is about 0.25 to 1.20 m thick (Ad, Table 1) are deposited on the DL facies and are interpreted as aeolian dunes (Ad, Table 1 and Fig. 7A, and 7B). The interbedded horizontally or low angle laminated sandstones, with well sorted and well rounded quartz, are up to 6 m thick and 2 km long, they represent aeolian sandsheet deposits (Ah, Table 1 and Fig. 7A) that. This facies association attributed to erg deposits is named ER (Table 3). The bounding surfaces between the individual sets of cross-strata are slightly dipping towards stoss side (Fig.7A). The palaeowind direction, from the aeolian dunes, is towards the WNW to NW (Fig. 6). The palaeowind direction was slightly oblique in comparison with the expansion direction of the alluvial fan deposits. The sandy ER facies association is more and less continuous laterally and overlies the fan sedimentation. Towards the west, 2 km from the Tanoumri section, the aeolian dunes and sand sheets evolved into grouped wedge-shaped cross-bedding and reveal similar dip directions of the foresets, and characterized grouped crescentic aeolian dunes

(Figs. 7C, and 7D) similar to those described in Spalletti et al., (2010), These facies associations from 0 to 28.5 m (F3a Subunit, Fig. 6), with only a few calcisols (Pc-II) characterize the proximal alluvial fan (AFp) at the base of the F3a Subunit and the mid-alluvial fan depositional environment, from the proximal (AFm1) to distal position (AFm2) within an erg environment (ER) in the arid alluvial plain.

From 28.5 to 35 m (Fig. 6) a new facies association appears, mainly composed of sandy facies (Sp, Sl, Sm and Shg) up to 1 m-thick, that displays flat based beds deposited by sheetflood events (sandflat bedforms), slightly modified by calcretes as circular to ovoid carbonate nodules (palaeosol Pc-II, Table 2) and by gleyed or mottled silty- or sandy-clay and carbonate beds, with redoximorphic concentrations (Pg hydromorphic soils, Table 2 and Fig. 4N, 4O, and 4P) and Fsm facies with laminar carbonates of mature calcisols (noted Pc-IV to VI, Fig. 6). This facies association represents distal alluvial fan deposits (AFd; Figs. 4N, and 4O) in a subhumid setting as shown by the palaeosol developments (AFd; Table 3). The AFd facies association is progressively vertically interbedded with carbonate facies (Cpa, Cpe facies, Table 1) and sandstone beds (Sq facies, Table 1). The carbonates of the Cpa facies are massive to laminated carbonates, with desiccation cracks and micritic intraclasts (Fig. 4O, and 4Q) typical of a phreatic setting (Alonso-Zarza, 2003). The depositional setting of these carbonates is characterized by a low energy lake margin (Alonso-Zarza and Wright, 2010) and is typical of palustrine carbonates with diversified paedogenic processes that introduce later transformations (roots, desiccation and paedogenic remobilizations, Freytet, 1984) (Cpe, Fig. 4R). The paedogenic carbonates (Cpe), interbedded with palustrine carbonates (Cpa), show paedogenic structures like alveolar-septal (Fig. 8A), vertical desiccation cracks and sparitic-coated grains that leads to the formation of calcisols (stages IV to VI in Machette 1985, Table 2). The associated sandstone beds (Sq, Table 1) are composed of sub- to rounded quartz grains with a polished and gleaming surface, and have no ocher yellow to reddish hue

(Fig. 8B). This characteristic suggests no pedogenetic influence (Ernest et al., 2019). The Sq facies characterizes aeolian grains reworked by the waves. This facies association (named PA, Table 3, and Fig. 4O) represents palustrine deposits with some sandstone beds, characterizing reworked aeolian deposits in waves along a lake. Interbedded with PA, a new facies association appears to be characterized by well (Gh, Sl facies) to moderately sorted (Gp facies) material and sub-angular to rounded intra- and extraclasts and two slightly opposite directions of bedding (Fig. 6, 8C, 8D, and 8E). This facies association, associated with the development of paedogenic calcrete (PC-III, Table 2), is up to 4-m thick and is characterized by a 200 m to 1 km lenticular shaped extension, with a flat base and convex top. It is interpreted as a gravel lake shoreline or berm, deposited at the marginal lake, along the distal fan (named Bm, Table 3, and Fig. 8 C). The beach face is characterized by Gh, Sl facies, fine material and low-angle foresets (Fig. 8C and 8D). The backshore is characterized by Gp facies, coarse material and relatively high-angle foresets (Fig. 8C and 8E). The berm deposits (Bm) are characterized by algal mats structures (AM, Table 1, and Fig. 8F), similar to those described by Chu et al. (2017, 2015), Paul et al. (2011), and Schieber et al. (2007). Two palaeocurrent directions are defined: one towards the NNE (dispersion angle of 100°) recorded by a relatively high angle bedding with medium-sized pebbles (Gp), and a second palaeodirection, towards the SSE, measured from the relatively low-angle interbedded fine pebble bedding (Gh) and from imbricated pebbles. This shoreline butte is sometimes emerged by the lake in humid conditions (Blair, 2000). The Tanoumri berm (Bm, Table 3) may be comparable to the shoreline butte of Manly Lake in Death Valley (Blair, 2000). The Tanoumri section shows two to three berms depending on the WSW-ENE position of the section. The Bm and PA facies associations of lacustrine shoreline and palustrine environments associated with Pg and Pc-III to VI soils (Table 2) attest to a subhumid climate.

Consequently, the F3 Unit is subdivided in two subunits (Fig. 6). The F3a Subunit is mainly composed of a mid-alluvial fan within an arid alluvial plain (AFm1 and AFm2), with desert pavement deposits (RE) and with increasingly developed erg deposits (ER). The palaeocurrent direction is towards the NNE to W and the palaeowind direction is towards the WNW to NW (Fig. 6). The F3b Subunit (Fig. 6) is characterized by a distal alluvial fan (AFd), within a palustrine environment (PA) and a well-developed berm at the top, within a semi-arid to subhumid climate evolution (Fig. 6).

The F4 Unit covers the F3 Unit, and it can be divided in two subunits named F4a and F4b from the base to top (Fig. 6). The F4b Subunit rests unconformably on the F4a Subunit with an angular unconformity (named BS2) that is well-defined on the outcrops (Fig. 5C). The F4a Subunit is mainly characterized by fine-grained sediments (Fm, Fl and mainly Fsm facies, Table 1) with fine to medium-grained sandstones to siltstones (Sp, Sh, Sr facies, Table 1) that are interbedded. The sandy to silty beds, up to 1.5 m-thick and more than 100 m long, display a flat base and a convex to irregular top (Fig. 8G) and local burrows (Sb2 Taenidium Barretti from Baucon et al. (2014), Buatois and Mángano (2004), and Gibert and Saez (2009), Table 1, Fig. 8H). The Fsm facies, with scattered carbonate nodules and mottling (Pg soil, Table 2, Fig. 6), represents alluvial plain deposits under a subhumid climate. This facies association (named FF, Table 3, and Fig. 8G) characterizes the terminal splays bedforms, flowing towards the NNE to NNW (Fig. 6), within a subhumid alluvial plain. These deposits evolve vertically to braided river deposits, and are called the RB facies association (Fig. 6).

Basal part of Middle Triassic depositional environments

The F4b Subunit rests unconformably on the F4a Subunit. The 9 m thick studied interval of the F4b Subunit (Fig. 6) displays fine-grained sediments, pedogenically altered (Fsm,

Table 1) and are interbedded with massive and monogenic conglomerates, mainly composed of reworked carbonate pebbles to granules (Gmi, Table 1). The facies association (Fsm, Gmi) represents floodplain deposits (FP, Table 3) interbedded with conglomerates massive and showing an erosive base of lag deposits (Gm, Table 1), followed by trough cross-bedded conglomerates, and formed by 3D dunes migration (Gt, Table 1).The sandstone part displays planar cross-bedding from 2D dunes migration (Sp, Table 1) and finally ripple cross-laminated sandstone (Sr, Table 1), associated sometimes with Scoyenia burrow (Sb1, Table 1; Frey et al., 1984; Gibert and Saez, 2009; Hasiotis, 1997). The Gm, Gt, Sp and Sr facies association up to 2.5 m-thick and more than 1 km long laterally represents point bar deposits of meandering river (named RM, Table 3).. The floodplain and meandering fluvial facies association with reworked calcretes (Gmi facies) and Pv soils (Table 2) characterizes a semi-arid climate.

4.2.2. Aït Tamlil section

The Aït Tamlil section is located in the eastern part of the MHA (Figs. 1B, 5D to 5F, 8I to 8Q, and 9).

Upper Permian depositional environments

In this section, the top of the upper Permian (F2 Unit; Fig. 9) is mainly characterized by sandstones (Sp, Sm, Sh, Sr; Table1) and fine-grained facies (Fm, Fl, Fsm; Table1) with several 4 cm- to 1m-thick conglomerates (Gp, Gh; Table1). The conglomerate and sandstone facies associations are 20 cm- to 1.70 m-thick and 15 to 100 m long, with a main palaeocurrent oriented to the SE (Fig. 9). Locally, some Sr facies display a palaeocurrent oriented to the N220 (Fig. 9) and they represent a 1.70 m-thick lateral splay that is oblique to perpendicular to the main current. These facies associations, displaying fining-upward sequences from terminal or lateral splays within alluvial plain deposits with calcic soils (Pv,

Pc-IV), are typical of a medial to distal fluvial fan (FF facies association, Table 3), characterizing thin broad and shallow distributary channels evolving into terminal splays deposits, within an arid to semi-arid climate (Fig. 9). The main stream flow is towards the SE.

Lower Triassic depositional environments

The F3 Unit (Fig. 9) rests in angular unconformity on the Permian strata (Fig. 5F, BS1). Up to 41.5 m thick, it is mainly composed of conglomerates (Gt, Gp, Gh, G/S, Ga, Table 1) and sandstone (Sg/S, Sm, Sp, Sh, Sr, So, Table 1) with aeolian (Ar, Ad, Ah, Table 1) and some mudstones and sandstones facies (Fm, Fl, Fsm, Sp, Sr, Sh, Table 1). Within this part of the section, the facies association is mainly characterized by med-alluvial fan depositional environments, from a proximal (AFm1, Table 3) to distal position (AFm3, Table 3) within an erg environment (ER, Table 3), and with some distal alluvial fan deposits (AFd, Table 3). The first Triassic bed, up to 1.5 m thick, is composed of reworked aeolian quartz (Gp, Sh facies with rounded quartz). The med-alluvial fan deposits (AFm1; Table 3; Fig. 9) are mainly composed of G/S, Ga, and Gm facies characterizing sheetflood events with planar gravelly-sandy couplets (G/S) and wedge-planar sandy-pebbles (Ga), with upfan wind sand (Ar). The more distal environment to AFm1, named AFm2 (Table 3; Fig. 9) is composed of mixed gravely stream flow deposits (Gt, Gp, Gh facies) evolving to sandstone facies (Sh, Sr, Sp, Sm). These med-alluvial fan deposits (AFm1, AFm2) are interstratified with aeolian sand sheets (Ah) or simple aeolian dunes (Ad) up to 40 cm-thick and up to 10 m long (ER; Table 3; Fig. 9), generated by a wind direction oriented towards the SW (Fig. 9).

From around 19 m (F3a-F3b boundary), the mature soils (Pc-IV) are increasingly developed (Fig. 8I and 8J) and we find a third facies association (AFm3) mainly composed of sandy couplets of Sg/S facies, up to 80 cm-thick, capped by Sm facies typical of sheetflood events (Fig. 9). This facies association (Table 3) represents the most distal med-alluvial fan

system with mature soils (Pc-IV, Table 2). This succession is capped by oolitic lacustrine deposits represented by superimposed L1 and L2 facies associations (Table 3, Fig. 8K), at the top of the F3b Subunit. L1 represents the lacustrine deposits characterized by interstratified oolitic limestone COl and COr facies (Table 1, Figs. 8K, 8L and 8M). The COl facies (Table 1) is a bed up to 3 m-thick and extending hundreds of meters, with a flat to undulatory base and a flat top (Figs. 8K and 8L). It is associated with algal mat structures or small stromatolites (AM, Table 1, Fig. 8N) (Buatois et al., 2013; Chu et al., 2015; Paul et al., 2011) and glistening/blunt to rounded quartz (Figs. 8K, and 8O). The lenticular COr facies (Figs. 8K, and 8M) displays laminated limestone with wave and current ripples (current towards a N110-120 direction) (Fig. 9) that revealed a N25 direction of the lake shoreline. The L1 facies association is characterized by a lack of mud cracks which supports a subaqueous deposition and it is interpreted as interstratified oolitic shoal and shoreface lobes (Milroy and Wright, 2002, 2000; Palermo et al., 2008; Voigt et al., 2011). The L2 facies association is represented by oolitic sandstones (So facies, Fig. 8O), the beds are up to 3 m thick and extend 40 m laterally, the base is flat and the top is irregular to convex. This stacked So facies is interstratified with Sh and Sr lithofacies to form lobes up to 5 m thick. The sorting planar stratification allows this facies association to be attributed to planar bed conditions produced by swash-backwash processes in foreshore lobes (Milroy and Wright, 2000; Palermo et al., 2008; Voigt et al., 2011). This F3b succession, from 19 m (Fig. 9), displays calcitic laminar horizons with sometimes deformed shape (Table 2, Stage IV of Machette, 1985). These thick mature soils (Pc-IV, Fig. 8J) are formed by repeated erosion, sedimentation, reworking and renewed calcrete formation (Alonso-Zarza et al., 1998), under a semi-arid climate. From 33.75 to 40.50 m (Fig. 9), the sandstone and mudstone host rocks show root traces and mottled horizons, associated to redoximorphic concentrations (Pg soils, Table 2 and Fig. 8K within AFd facies association). The mainly poorly drained soils (Pg), indicating a rise in the

ground water level and water-logging, attested to by redoximorphic alterations (Gleization) (Retallack, 2001; Tabor et al., 2006; Tabor and Montañez, 2004), within a subhumid alluvial plain (Fig. 9).

As a result, the F3 Unit can be subdivided in two subunits. The lower part of the F3 Unit association (F3a Subunit, Fig. 9), until around 19m, represents a med-alluvial environment with an ephemeral stream within an arid alluvial plain. The palaeocurrents were oriented towards the N100-230 with a dispersion angle of 130° (Fig. 9). The upfan currents (Fig. 9) were oriented in a N300-315 direction, measured from the backsets (Ga) and aeolian drift (Ar) lithofacies. The prevailing wind was towards the SW (Fig. 9) generating simple aeolian dunes. The F3b Subunit also represents a med-alluvial to distal fan system, evolving towards the top to a distal alluvial fan (AFd). The F3b preferential palaeocurrents were towards the ESE to SE, measured from the planar cross-bedding of the gravel bars (Gp facies). However, the planar cross-beddings of the backsets (Ga facies) give upfan currents towards the WNW.

These deposits evolve to the F4 Unit which is divided into two subunits: F4a and F4b (Fig. 9), separated by an angular unconformity (Figs. 5F, and 8P). The F4a Unit, 29 m-thick, mainly consists of mudstones (Fm facies) with stromatolites (AM facies) and scattered oolites, and a few sandstone beds (Flo facies). Some lenticular oolitic beds are concentrated at the base of this interval and are more or less absent thereafter. These laterally extensive mudstone successions are interpreted as a coastal plain or strand plain (Milroy and Wright, 2002, 2000) and are attributed to the L3 facies association (Table 3; Figs. 8P, and 9). The F4a Subunit evolves vertically to the St, Sm and Sr facies, which characterize bedload sandy bedforms attributed to a med-alluvial fan (AFm2 facies association; Table 3 and Fig. 9).

Basal part of Middle Triassic depositional environments

The F4b Subunit rests in angular unconformity on the F4a Subunit (Figs. 5F and 8P). The 12 m studied interval of the F4b Subunit (Fig. 9) displays meandering river and floodplain deposits (RM, FP facies association; Table 3, and Fig. 8Q) under a semi-arid climate, with the same facies and facies association as the F4b Subunit in the Tanoumri section (Fig. 6). The difference lies in the thickness of the sedimentary bodies, which are thicker in the Aït Tamlil section. The palaeocurrent of the meandering river is mainly to N210 (Fig. 9).

5. Depositional environment evolution and sequence stratigraphy from the Permian-Triassic unconformity to the Middle Triassic

In the High Atlas, an angular unconformity (named BS1) is observed everywhere between the Permian and Triassic successions (Baudon et al., 2012). The upper part of the Permian in the Argana (t2 Unit) and MHA (F2 Unit) basins is illustrated by three sections (Irerhi, Tanoumri and Aït Tamlil; Figs, 1B, 2, 3, 5, 6, and 9). During the late Permian, these three sections show distal fluvial fan deposits (FF) with calcisols (Pc-II, Pc-IV soils, rarely Pc-VI), calcic vertisols (Pv soil) and hydromorphic soils-gleying (Pg soil) which are typical of a semi-arid climate. Unlike the other sections, Tanoumri displays an interbedded palustrine deposit (PA). However, the palaeoenvironmental evolutions from the Lower to Middle Triassic succession through the three basins are different.

5.1. Argana Basin

The base of the t3 Unit, overlies the P-T unconformity (Fig. 1C) is characterized by a widespread palaeo-desert pavement induced by a long hiatus in sedimentation (Durand and Bourquin, 2013), overlain by mainly alluvial fan deposits dated as Olenekian (Klein et al., 2010; Tourani et al., 2010). These first depositional environments, i.e., the t3a Subunit (Fig. 2), reflect arid conditions as indicated by the ephemeral stream evolving from proximal to med-distal alluvial fan, associated with mature paedogenic calcretes (Pc). The t3b Subunit is

characterized by distal alluvial fan and floodplain deposits with mixed hydromorphic soils-gleying (Pg soil) and mature calcretes (Pc-V), with semi-arid/subhumid climate evolution The upper part of the t3b Subunit displays well-extend braided river deposits, overlain by the distal alluvial fan of the t4a Subunit. This Subunit, dated as Olenekian, shows an evolution to a more humid climate with the development of only hydromorphic soils-gleying (Pg soil) (Fig. 2). Moreover, the Lower Triassic succession, i.e., the t3a, t3b and t4a subunits, is characterized by a general retrogradational trend until a maximum flooding surface (MFS) and progradational trend that ends with a regional unconformity between the t4a and t4b subunits (named BS2, Fig. 2). The maximum flooding is characterized by well-extended floodplain deposits at the Argana Basin scale. The 6 m lowermost part of the t4b Subunit, dated as Anisian, characterizes the beginning of a new retrogradational trend displaying floodplain deposits with calcic vertisols formed under seasonally dry conditions in a semi-arid climate evolving to pond environments which outcrop above the upper limit of Irerhi section (outside the scope of this study).

5.2. Marrakech High Atlas basins

In the MHA, the evolution of the palaeoenvironment from the Lower to early Middle Triassic is illustrated using the Tanoumri and Aït Tamlil sections (Figs. 1B, 1C, 5, 6, and 9).

5.2.1. Tanoumri section

Above the P-T unconformity (BS1, Fig. 6), the Triassic series begins with widespread palaeoreg deposits as observed in the Argana Basin, overlain by med-alluvial fan deposits with interbedded dunes and interdunes and thin alluvial plain deposits characterized by immature calcisols. Above a second level of palaeo-desert pavement deposits, the aeolian bedforms are more developed than the med-alluvial fan. These deposits (F3a Subunit, Fig. 6) attest to a period of arid climate conditions interbedded with a long sedimentation hiatus,

without any vegetation, as indicated by the palaeoreg developments. Above F3a, the F3b Subunit is composed of a distal alluvial fan and displays hydromorphic soils-gleying and mature calcic soils in a semi-arid/subhumid climate evolving to palustrine deposits and shoreline lake deposits. These deposits characterized the maximum rise of the water table, and evolved vertically to distal fluvial fan, associated with hydromorphic soils-gleying in a subhumid climate (F4a Subunit). An angular unconformity (named BS2, Fig. 5C, 6) tops the F4a Subunit. Consequently, the Lower Triassic succession, i.e., F3a, F3b and F4a, is characterized by a general arid retrogradational trend, from proximal alluvial fans to lacustrine-palustrine distal environments and a semi- arid to subhumid progradational trend. This part of major cycles ends with the angular unconformity between the F4a and F4b subunits (Fig. 6). The maximum flooding is characterized by lacustrine shoreline deposits. The progradational trend is characterized by an evolution from lacustrine to fluvial deposits always in subhumid climate conditions. The F4b Subunit, attributed to the Middle Triassic, exhibits a meandering system with a well-developed floodplain showing calcic vertisols under seasonally dry conditions in a semi-arid climate. This lowermost part of the Anisian age displays relatively a proximal to medial fluvial system, and evolves to pond deposits from other field work data outside the scope of this study, in a new retrogradational cycle.

5.2.2. Aït Tamlil section

In the Aït Tamlil section, above the P-T unconformity (BS1, Figs. 5F and 9), the lower part of the F3 Unit (F3a Subunit, until 18.5 m) is mainly characterized by med-alluvial fan deposits interbedded with aeolian and alluvial plain deposits without a palaeosol at the base and with immature calcisols in its upper part. This depositional environment attests to an arid climate. These deposits evolve vertically to a med-alluvial fan with rare aeolian deposits and then to a distal alluvial fan with mature and immature calcisols, hydromorphic soils, oolitic shoal and shoreface lobe deposits from a lacustrine environment (F3b Subunit). This

evolution and palaeosol developments attest to semi-arid to subhumid climate conditions. The F4a Subunit is characterized by a vertical evolution from a coastal plain and then to med-alluvial fan deposits limited at their top by a tectonically-induced angular unconformity (BS2, Fig. 5F). As a result, the Lower Triassic succession, i.e., the F3a, F3b and F4a subunits, is characterized by a general retrogradational and progradational trend that ends with the BS2 unconformity (Fig. 9). The maximum flooding is characterized by oolitic shoal and shoreface lobes. The F4b Subunit shows the beginning of a new retrogradational trend from a floodplain with meandering rivers to pond deposits under a semi-arid climate.

6. Correlation and palaeoenvironmental reconstructions in the High Atlas basins

6.1. Correlation between the Argana and Marrakech High Atlas basins

Based on the depositional environments and the unconformities identified in this work, a correlation between the Argana Basin and the MHA basins is established. During the late Permian (t2/F2 units), the basin is filled by distal fluvial fan deposits as terminal splays interbedded within floodplain deposits where the palaeosols indicate a semi-arid to arid climate under contrasting dry/wet seasons. In the Argana Basin, the fluvial fan systems flow to the NW while in the MHA basins the palaeocurrents flow to the NNW or to the NE, in the Tanoumri area, and to the SE and rarely to the SW in the Aït Tamlil area, attesting to independent basins in the High Atlas during the late Permian. The angular unconformity above the late Permian overlain by the flat Triassic series indicates that these Permian basins were tilted then eroded.

Above the P-T unconformity (BS1, Figs 2, 3, 5, 6, and 9), in the High Atlas basins, the depositional environments are always characterized by arid environments that evolve vertically to semi-arid/subhumid conditions. Based on the boundary surfaces, the climate evolution and the available biostratigraphic constraints figure 10 proposes a correlation

between High Atlas three basins. The first Triassic sediments are preserved as a palaeoreg surface (ventifacts) and a few ephemeral med-alluvial fan deposits (t3a Subunit, Fig. 2) in the Argana Basin whereas in the MHA basins, during this arid episode, an ephemeral alluvial fan within erg deposits and sometimes palaeo-desert pavement surfaces are preserved (F3a Subunit, Figs. 6, 9, 10). During this episode, in the Argana Basin, the series are thinner and without aeolian dune preservation, this could indicate more sedimentation gap with probably more desert pavement deposit preservation (Fig. 10). The depositional environments evolve progressively to semi-arid/subhumid climate conditions in the Argana (t3b and t4a subunits) Basin and in the MHA (F3b and F4a subunits) basins (Fig. 10). In these three areas, we observed a retrogradational trend until a well-extended floodplain (Argana) or lake deposits (Marrakech High Atlas) which mark a maximum flooding episode (denoted MFS, Figs. 2, 6, 9, and 10). The progradational trend is marked by a large extension of the fluvial or alluvial deposits (Fig. 10), until an angular unconformity between the Lower and Middle Triassic (BS2, Figs 2, 6, and 9). Above this unconformity, the climate becomes semi-arid and the alluvial plain with meandering river to pond deposits is recorded in the Argana and High Atlas basins (t4b and F4b respectively, Fig. 10).

6.2. Palaeoenvironmental reconstructions in Marrakech High Atlas basins

The Argana Basin seems to be separated from the MHA basins, by a topographic high "Massif Ancien" (Fig. 1B) during the Triassic (Domènech et al., 2015; Mader and Redfern, 2011; Ouanaimi, 1989; Perez et al., 2019; Van Houten, 1977). The Triassic history of the MHA basins is more complex. From the sedimentological analysis of the Tanoumri and Aït Tamlil areas, four palaeoenvironmental reconstructions can be established for the Early Triassic (Fig. 11), to show the evolution of these two disconnected basins during the Early Triassic. Within the Tanoumri area, the palaeoenvironmental reconstruction during the arid period (Fig. 11A, 11B) can be used to show alluvial fan deposits located to the SE along N30

normal faults that evolve into erg deposits towards the NW with well-developed aeolian dunes (Fig. 7). The alluvial fan displays currents mainly towards the NNE to W (N30 to N280) (Figs. 6 and 11B). After a well-extended second palaeo-desert pavement (middle part of the F3a Subunit, Figs. 6), the aeolian deposits are more developed in this area. The aeolian dunes were deposited by the dominating winds blowing towards the NW to WNW (Figs. 6 and 11B). The sedimentary basin was limited, in the NW part, by a N70 border fault called the Anrar Fault (Vogel et al., 1980). The overlying depositional environment dominated by semi-arid/subhumid climate conditions (Figs. 6 and 11C) shows the following changes in the depositional profile: (1) a distal alluvial setting, (2) hydromorphic soils-gleying and mature calcic soils, (3) a palustrine and gravel lake shoreline with local lacustrine deposits. Around the lacustrine environment, the palaeocurrents are mainly oriented towards the NNE at the backshore and towards the SSE at the beach face. The estimated coalesced fans size is approximately 5 km wide.

Within the Aït Tamlil area (Figs. 9 and 11A), the arid period (F3a Subunit, Fig. 11D) is characterized by fans flowing towards the ESE up towards the SW, converging to the erg depocenter in the SE. The main blowing winds record a SW palaeocurrent direction. The sedimentary basin was limited, in the SE part, by a N70 border fault called the Tizi-n-Iblouzene Fault (Jenny, 1983; Jenny et al., 1989). The fan systems are represented by a flat base and convex top shape that is well exposed in the Aït Tamlil outcrops. The overlying semi-arid/subhumid period (F3b Subunit, Fig. 11E) is characterized by the drainage of the alluvial fan towards the SW to ESE. In the more distal zone, in the SE part of the basin, the distal alluvial fan evolved into extended lake facies. The lacustrine shoreline was elongated along a NE-SW direction, as attested to by wave and current ripples. Within the Aït Tamlil area, 10 km wide coalesced fans and a simple 70 to 500 m wide fan are observed.

In these two areas (Tanoumri and Aït Tamlil) above the well-extended lake, fluvial to alluvial deposits (F4a Subunit, Figs. 6, 9, and 10) prograde in the basin with basically the same palaeocurrent direction as the underlying alluvial fan deposits (Fig. 11). The sedimentation boundaries of the F4a Subunit in these two areas are unknown due to the post-Triassic erosion and therefore cannot be mapped in the MHA.

In the Argana and MHA basins, an angular unconformity (BS2) is observed at the top of the fluvial to alluvial deposits of t4a/F4a subunits (Figs. 2, 6, 9, and 10). As a result, the basal part of the Middle Triassic deposits, i.e., Anisian t4b/F4b subunits, rest unconformably on the t4a/F4a subunits. In the Argana Basin, the Anisian axial drainage was parallel to the N-S border fault (Fig. 3A). In the Tanoumri and Aït Tamlil areas, the Anisian deposits (F4b) represented an axial floodplain, where the rivers flowed towards the SW to WSW and towards the N210 (SW to SSW), respectively (Figs. 6 and 9). These palaeocurrents are oblique to parallel to the N70 border fault, limiting the Tanoumri Basin at its NNW part (Figs. 11B, 11C) and the Aït Tamlil Basin at its SSE part (Figs. 11D, 11E). The meandering rivers of the two basins flowed more or less parallel to the N70 axial valley. This change in palaeo-drainage, from transverse during the Early Triassic to axial during the Middle Triassic, is possibly related to a tectonic movement induced by the BS2 angular unconformity. Consequently, after the BS2 unconformity, the Aït Tamlil and Tanoumri basins may have been connected and together could have formed a large basin; however these basins still seem to be disconnected from the Argana Basin by the "Massif Ancien" high (Fig.1B). Moreover, F4 Unit is only characterized by fluvial system without any tidal influence in accordance with Mattis (1977).

To conclude, during the Early Triassic, the Aït Tamlil and Tanoumri areas were two distinct basins (Fig. 1B) until the upper F4a Subunit. In the F4b Subunit, the basins became

connected (during the Anisian). The Argana Basin remains disconnected from the MHA basins throughout the Early and Middle Triassic.

7. Discussion

Comparison with European basins

To compare with the northwestern peri-Tethyan domain, figure 12 proposes a correlation between Moroccan and certain European basins. Almost everywhere in Europe, except in the central part of the Germanic Basin, a more or less angular unconformity is observed between the Permian and Triassic (Fig. 12). Induan sediments are only preserved in some parts of the Germanic Basin and record the same semi-arid climate condition of the late Permian (e.g., Bourquin et al., 2011; Ravidà et al., 2022). Mesozoic sedimentation at the European scale began in the early Olenekian. During this period (e.g., Bourquin et al., 2011; Galán-Abellán et al., 2013; Linol et al., 2009; Ravidà et al., 2022), palaeoenvironments were composed of either poorly preserved palaeo-desert pavement or reg deposits (i.e., Devon, SE France, Balearic Islands) or regs and aeolian dunes (e.g., France, Germanic Basin, Iberian Range), with sometimes, in the central part of the Germanic Basin, a playa-lake without evaporites (e.g., Bachmann et al., 2010). This playa-lake is controlled by a water supply coming from the adjacent relief (Bourquin et al., 2006; Péron et al., 2005). The Lower Triassic deposits record arid climate condition in the Moroccan basins, i.e., the t3a and F3a subunits, and could be a time equivalent of the arid climate condition described in European basins considered as Olenekian in age (Fig. 12). In Europe, the Olenekian arid deposits evolve vertically into well-developed fluvial deposits recording a semi-arid environment with the first occurrence of palaeosol developments dated as Spathian in the Germanic Basin (Szurlies 2007; Fig. 12). At the margin of this basin or in some other basins, a major hiatus of sedimentation is observed, sometimes underlined by palaeosol developments (i.e., Paris Basin, Balearic Islands, Fig. 12).

However, in southern Europe, Olenekian arid conditions continue until the late Spathian (e.g., Iberian Range; Galán-Abellán et al., 2013). The Spathian deposits with palaeosol developments could be equivalent to the t3b, t4a and F3b, F4a subunits in the High Atlas (Fig. 10), which display a similar evolution to semi-arid conditions (Fig. 12).

In Europe, an erosional unconformity, called the Hardegsen unconformity, is observed almost everywhere (Fig. 12) and is dated as intra-Spathian in the Germanic Basin (Geluk and Röhling, 1997; Szurlies, 2007). Above this unconformity, the Anisian-Ladinian deposits evolve vertically to fluvial deposits recording a semi-arid climate which transitions to open marine sedimentation during the Muschelkalk Sea transgression in distal areas (e.g., Bourquin et al., 2011; Lloret et al., 2021; McKie and Shannon, 2011). In northern European basins, multiple unconformities are observed during this period and the Anisian-Ladinian deposits are characterized by fluvial with some aeolian deposits in separated basins episodically connected to the marine base level, with land-locked playa or evaporite salinas (e.g., McKie and Shannon, 2011). The BS2 unconformity observed in Moroccan basins could be the time equivalent of the unconformities observed in European basins, i.e., late Olenekian-early Anisian (Fig. 12).

Tectonic control

In the northwestern and southwestern peri-Tethyan domain, the P-T transition is characterized by an angular unconformity, classically attributed to a final orogenic collapse phase (Burg et al., 1984; Leleu et al., 2016; Lorentz and Nicholls, 1976; Ménard and Molnar, 1988; Redfern et al., 2010) or regional uplift, preceding Triassic rifting and the break-up of Pangea related to the opening of the Tethys and Atlantic Oceans (Charton et al., 2020; Ziegler and Dèzes, 2006). However, the angular nature of the Base Triassic unconformity (Baudon et al., 2012) and the Lower Triassic by-pass through the continental domain and the change in the fluvial

network between the Permian and Triassic indicate a period of relief rejuvenation during the late Permian (Bourquin et al., 2011; Ravidà et al., 2022). Moreover, in the northern European domain where a transition is observed with Induan sediment preservation (Bourquin et al., 2011; McKie and Shannon, 2011; Scholze et al., 2017), a late Permian to Early Triassic extension and fault block rotation have been observed and attributed to an early rifting episode (Eide et al., 2018; McKie and Shannon, 2011). In Moroccan basins, the P-T unconformity is also a matter of debate (Baudon et al., 2012), from relaxation or collapse of the chain (Saber et al., 2007) or pronounced crustal thinning and regional uplift before Triassic rifting (Manspeizer et al., 1978). Like in Europe, this P-T unconformity can be interpreted to have created topography with different sedimentation areas: desert pavement deposits in the high topographies (Argana basin) and desert pavement and aeolian dune preservations in the low topographies (Tanc[illegible]ri Aït-Tamlil basins) overlain by fluvial-lacustrine deposits. These topographies seemed to be progressively infilled until a new period of structural re-organisation, in the upper Early Triassic, recognized in Europe, i.e., the Hardegsen unconformity, as well as in High Atlas basins. This intra-Spathian unconformity observed in the northwestern peri-Tethyan domain (Fig. 12) is attributed to a significant structural reorganization linked to the onset of extensional tectonics and the ongoing break-up of Pangea (e.g., Galán-Abellán et al., 2013; Geluk, 2005; Geluk and Röhling, 1997). This tectonic phase could be the time equivalent of the BS2 unconformity recorded in the Moroccan basins of the High Atlas, defined for the first time in this Gondwana domain. In the European domain, this structural reorganization leads to new source areas and a new fluvial style under marine influences at the distal part of the system (e.g., Bourquin et al., 2011; Galán-Abellán et al., 2013). In Moroccan basins, this unconformity led to a restructuration of the Triassic basins with a change in the palaeo-drainage (Figs. 6, 9). Based on this study, integrated with previous tectonic studies (Arboleya et al., 2004; Baudon et al., 2009;

Beauchamp, 1988; Beauchamp et al., 1996; Domènech et al., 2018, 2015; El Arabi et al., 2006b, 2003; Frizon de Lamotte et al., 2015, 2009; Laville et al., 2004; Leleu et al., 2016; Missenard et al., 2007; Moragas et al., 2017; Oliva-Urcia et al., 2016; Redfern et al., 2010), several composite basins have been recognized in the MHA; they were probably connected during the early Middle Triassic after the BS2 unconformity. It appears that the Argana Basin was always separated from the MHA basins, where the t4 Unit records an extension of sedimentation across the entire Argana Basin (Leleu et al., 2016). This extension is the intra-t4 Unit and begins above the BS2 unconformity and can be compared to the reorganization of sedimentation in the MHA basins.

Climate

The late Permian strata is characterized in the Argana Basin by palaeosols representing a paleolatitudinal transect of ~ 5°N with an estimated MAP (Mean Annual Precipitation) average of 27 ± 5 cm, which indicates that these were the driest conditions (Tabor et al., 2017). This study, in the MHA and Argana basins, reveals vertic calcisols, calcic vertisols and occasionally hydromorphic soil gleying thereby indicating an arid to semi-arid climate.

During the Early Triassic, it is considered that cooler phases occurred in the early Smithian, with a period of extreme warmth in the middle or late Smithian associated with ecological changes in the floral composition and a high faunal taxonomic turnover in the ocean (e.g., Goudemand et al., 2019; Romano et al., 2013). A new cooler episode characterized the beginning of the Spathian with palaeosol developments and preservation of footprints in the Central Pangea (e.g., Romano et al., 2013). This Smithian Triassic global warming is characterized by exceptionally high values (Péron et al., 2005; Sun et al., 2012). During the basal part of the Early Triassic, i.e., Induan, when sediments are preserved they reflect the same semi-arid condition as observed in the late Permian. This Induan age is

claimed to be missing in the three sections, and the early Lower Triassic (t3a and F3a subunits) started with a very hot climate condition with widespread palaeoreg and aeolian preservation. These desert sedimentary facies are observed in Europe and Morocco and are probably considered as middle to late Smithian age.

As a result, during the Early-Middle Triassic, the climate evolution in the northwestern and southwestern peri-Tethyan domain is from a semi-arid, i.e., Induan, to arid, i.e., Smithian, and semi-arid environment, i.e., Spathian.

8. Conclusion

The late Permian, Early Triassic and basal part of the Middle Triassic represent the studied age range, in Irerhi section (Argana Basin, t2 Unit, t3a, t3b, t4a, and t4b subunits) and in Tanoumri and Aït Tamlil sections (Marrakech High Atlas basins, F2 Unit, F3a, F3b, F4a, and F4b subunits). According to new sedimentological data, the Upper Permian to Lower Triassic deposits are characterized by changes in the (1) environments, i.e., respectively fluvial fan in t2 / F2 units and palaeoreg with ventifacts, followed by proximal to med-alluvial fan deposits in t3a / F3a subunits that are associated to well-developed aeolian dunes (F3a), (2) palaeocurrent directions i.e. drainage direction changes by 10° to 15° depending on the basin, induced by P-T angular unconformity (BS1), and (3) palaeosol types i.e., respectively mainly vertisols and hydromorphic soils-gleying involving an arid to semi-arid climate within the late Permian (t2 / F2 units) and calcisol / aridisol formed in an arid climate during the early Lower Triassic (t3a / F3a subunits). These arid depositional environments evolve vertically to more humid conditions within the distal-med-alluvial fan and well-developed floodplain or lacustrine deposits (t3b and t4a / F3b and F4a) with vertisol, mature calcretes and hydromorphic soil-gleying. Moreover, in the three sections, the same evolution from a retrogradational and then progradational trend is observed. Its upper part displays well-

extended fluvial or alluvial fan deposits, and ends by a tectonically induced angular unconformity (named BS2), identified for the first time. Above the BS2 unconformity, the depositional environments dated as Anisian (t4b / F4b subunits) are characterized by a meandering river in a semi-arid floodplain. The palaeoenvironmental reconstructions, show that sedimentation in the High Atlas were recorded in numerous independent Lower Triassic basins. Above the P-T boundary and remnant topographies, different sedimentation areas are observed with only reg deposits in the high topographies (Argana Basin) and reg deposits and aeolian dunes in the low topographies (Tanoumri, Aït Tamlil basins), associated with ephemeral alluvial fan deposits with various transverse palaeocurrent and oblique palaeowind directions, controlled by N70 border faults. In Tanoumri Basin, the fans palaeocurrent directions are towards the NNE to W and palaeowind towards the NW to WNW. In Aït Tamlil Basin, the alluvial fans flow towards the ESE up towards the SW and the blowing winds are to SW direction. These arid deposits are overlain by fluvial and lacustrine sediments in more humid climate conditions (F3b subunit). After the BS2 angular unconformity, an axial palaeo-drainage is observed and the Aït Tamlil and Tanoumri basins were probably connected but always disconnected from the Argana Basin.

Compared with Western Europe, the arid climate period recorded in High Atlas Lower Triassic (t3a / F3a subunits) corresponds to the early Olenekian (Smithian), whereas the semi-arid to subhumid period (t3b, t4a / F3b, F4a) corresponds to the late Olenekian (Spathian), and the BS2 unconformity could correspond to the Hardegsen discontinuity. These results show the same climate evolution in western terrestrial Tethys basins, i.e., North Gondwana and European, reflecting a global climate evolution. Moreover, the tectonically induced unconformities observed in these two areas have called into question the timing of the rifting in Morocco and Europe related to the opening of the Atlantic Ocean.

Acknowledgements

This work was logistically supported by the Cadi Ayyad University, Faculty of Sciences Semlalia-Marrakech. This publication received financial support from the MNHN-PPF 04 project "Biodiversité actuelle et fossile. Crise, stress, restaurations et panchronisme: le message systématique". The authors thank Sara Mullin for proofreading the English content. They also thank the reviewer Zhicai Zhu and the anonymous reviewer for improving the final version with their pertinent comments.

References

Aït Chayeb, E.H., Youbi, N., El-Boukhari, A., Bouabdelli, M., Amrhar, M., 1998. Le volcanisme permien et mésozoïque inférieur du bassin d'Argana (Haut-Atlas occidental, Maroc): un magmatisme intraplaque associé à l'ouverture de l'Atlantique central. J. African Earth Sci. 26, 499–519. http://doi.org/10.1016/S0899-5362(98)00029-3

Alonso-Zarza, A.M., 2003. Palaeoenvironmental significance of palustrine carbonates and calcretes in the geological record. Earth-Science Rev. 60, 261–298. https://doi.org/10.1016/S0012-8252(02)00106-X

Alonso-Zarza, A.M., Calvo, J.P., 2000. Palustrine sedimentation in an episodically subsiding basin: The Miocene of the northern Teruel Graben (Spain). Palaeogeogr. Palaeoclimatol. Palaeoecol. 160, 1–21. https://doi.org/10.1016/S0031-0182(00)00041-9

Alonso-Zarza, A.M., Silva, P.G., Goy, J.L., Zazo, C., 1998. Fan-surface dynamics and biogenic calcrete development: Interactions during ultimate phases of fan evolution in the semiarid SE Spain (Murcia). Geomorphology 24, 147–167. https://doi.org/10.1016/S0169-555X(98)00022-1

Alonso-Zarza, A.M., Sopena, A., Sanchez-Moya, Y., 1999. Contrasting palaeosol development in two different tectonic settings: the Upper Buntsandstein of the Western Iberian Ranges, Central Spain. Terra Nov. 11, 23–29. https://doi.org/10.1046/j.1365-3121.1999.00218.x

Alonso-Zarza, A.M., Wright, V.P., 2010. Palustrine Carbonates, in: Alonso-Zarza, A.M., Tanner, L.H. (Eds.), Carbonates in Continental Settings: Facies, Environments and Processes, Developments in Sedimentology. Elsevier, pp. 103–131. https://doi.org/10.1016/S0070-4571(09)06102-0

Arboleya, M.L., Teixell, A., Charroud, M., Julivert, M., 2004. A structural transect through the High and Middle Atlas of Morocco. J. African Earth Sci. 39, 319–327. https://doi.org/10.1016/j.jafrearsci.2004.07.026

Arzani, N., 2005. The fluvial megafan of Aparkoh basin (Central Iran): an example of flash-flood sedimentation in arid lands. In: Harvey, A.M., Mather, A.E. & Stocks, M. (eds). Alluvial Fans: Geomorphology, Sedimentology, Dynamics. Geol. Soc. London, Spec. Publ. 251, 41–59.

Bachmann, G.H., Geluk, M., Warrington, G., Becker-Roman, A., Beutler, G., Hagdorn, H., Hounslow, M., Nitsch, E., Röhling, H.-G., Simon, T., Szulc, A., 2010. Triassic, in: Doornbal, H., Stevenson A., A. (Eds.), Petroleum Geological Atlas of the Southern Permian Basin Area. EAGE, pp. 148–173.

Baucon, A., Ronchi, A., Felletti, F., Neto de Carvalho, C., 2014. Evolution of Crustaceans at the edge of the end-Permian crisis: Ichnonetwork analysis of the fluvial succession of Nurra (Permian-Triassic, Sardinia, Italy). Palaeogeogr. Palaeoclimatol. Palaeoecol. 410, 74–103. https://doi.org/10.1016/j.palaeo.2014.05.034

Baud, A., Atudorei, V., Sharp, Z., 1996. Late Permian and Early Triassic evolution of the Northern Indian margin: carbon isotope and sequence stratigraphy. Geodin. Acta 9, 57–77. https://doi.org/10.1080/09853111.1996.11105278

Baudon, C., Fabuel-Perez, I., Redfern, J., 2009. Structural style and evolution of a Late Triassic rift basin in the Central High Atlas, Morocco: controls on sediment deposition. Geol. J. 44, 677–691. https://doi.org/10.1002/gj.1195

Baudon, C., Redfern, J., Van Den Driessche, J., 2012. Permo-Triassic structural evolution of the Argana Valley, impact of the Atlantic rifting in the High Atlas, Morocco. J. African Earth Sci. 65, 91–104. https://doi.org/10.1016/j.jafrearsci.2012.02.002

Beauchamp, J., 1988. Triassic sedimentation and rifting in the High Atlas (Morocco). Dev. Geotecton. 477–497. https://doi.org/10.1016/B978-0-444-42903-2.50025-7

Beauchamp, J., Petit, J.P., 1983. Sédimentation et taphrogénèse triasique au Maroc: l'exemple du Haut Atlas de Marrakech. Bull. Centres Rech. Explor. Prod. Elf-Aquitaine 7, 389–397.

Beauchamp, W., Allmendinger, R.W., Barazangi, M., Demnati, A., El Alji, M., Dahmani, M., 1999. Inversion tectonics and the evolution of the High Atlas Mountains, Morocco, based on a geological-geophysical transect. Tectonics 18, 163–184.

Beauchamp, W., Barazangi, M., Demnati, A., El Aji, M., 1996. Intracontinental Rifting and Inversion: Missour Basin and Atlas Mountains, Morocco. Am. Assoc. Pet. Geol. Bull. 80, 1459–1482. https://doi.org/https://doi.org/10.1306/64ed9a60-1724-11d7-8645000102c1865d

Benaouiss, N., Courel, L., 1993. Oukaimeden Sandstone, Upper Triassic of High Atlas of Marrakesh: Tidal deposits, fluvial and alluvial fan., in: Field Guide, 14th IAS Regional Meeting of Sedimentology, Marrakesh, 27-29 April, 1993. pp. 157–179.

Benison, K.C., Goldstein, R.H., 2001. Evaporites and siliciclastics of the Permian Nippewalla Group of Kansas, USA: A case for non-marine deposition in saline lakes and saline pans. Sedimentology 48, 165–188. https://doi.org/10.1046/j.1365-3091.2001.00362.x

Bertrand, H., Dostal, J., Dupuy, C., 1982. Geochemistry of early Mesozoic tholeiites from Morocco. Earth Planet. Sci. Lett. 58, 225–239. https://doi.org/https://doi.org/10.1016/0012-821X(82)90196-0

Biron, P., 1982. Le Permo-Trias de la région de l'Ourika (Haut-Atlas de Marrakech , Maroc) : lithostratigraphie , sédimentologie , tectonique et minéralisations .

Blackburn, T.J., Olsen, P.E., Bowring, S.A., McLean, N.M., Kent, D.V., Puffer, J., McHone, G., Rasbury, E.T., Et-Touhami, M., 2013. Zircon U-Pb Geochronology Links the End-Triassic Extinction with the Central Atlantic Magmatic Province. Science (80-.). 340, 941–945. https://doi.org/https://doi.org/10.1126/science.1234204

Blair, T.C., 1987. Sedimentary processes, vertical stratification sequences, and geomorphology of the Roaring River alluvial fan, Rocky Mountain National Park, Colorado. J. Sediment. Petrol. 57, 1–18. https://doi.org/https://doi.org/10.1306/212F8A8A-2B24-11D7-8648000102C1865D

Blair, T.C., 1999a. Sedimentology of the debris-flow-dominated Warm Spring Canyon alluvial fan, Death Valley, California. Sedimentology 46, 941–965. https://doi.org/10https://doi.org/10.1046/j.1365-3091.1999.00260.x.1046/j.1365-3091.1999.00260.x

Blair, T.C., 1999b. Sedimentology of gravelly Lake Lahontan highstand shoreline deposits, Churchill Butte, Nevada, USA. Sediment. Geol. 123, 199–218. https://doi.org/10.1016/S00https://doi.org/10.1016/S0037-0738(98)00138-937-0738(98)00138-9

Blair, T.C., 2000. Sedimentology and progressive tectonic unconformities of the sheetflood-dominated Hell's Gate alluvial fan, Death Valley, California. Sediment. Geol. 132, 233–262. https://doi.org/https://doi.org/10.1016/S0037-0738(00)00010-5

Blair, T.C., McPherson, J.G., 1994. Alluvial Fan Processes and Forms, in: Geomorphology of Desert Environments. Springer Netherlands, pp. 354–402. https://doi.org/https://doi.org/10.1007/978-94-015-8254-4_14

Blair, T.C., McPherson, J.G., 1998. Recent debris-flow processes and resultant form and facies of the dolomite alluvial fan, Owens Valley, California. J. Sediment. Res. 68, 800–818. https://doi.org/https://doi.org/10.2110/jsr.68.800

Bourquin, S., Bercovici, A., López Gómez, J., Diez, J.B., Broutin, J., Ronchi, A., Durand, M., Arché, A., Linol, B., Amour, F., 2011. The Permian–Triassic transition and the onset of Mesozoic sedimentation at the northwestern peri-Tethyan domain scale: Palaeogeographic maps and geodynamic implications. Palaeogeogr. Palaeoclimatol. Palaeoecol. 299, 265–280. https://doi.org/10.1016/J.PALAEO.2010.11.007

Bourquin, S., Durand, M., Diez, J.B., Broutin, J., Fluteau, F., 2007. The permian-triassic boundary and lower triassic sedimentation in western European basins: An overview. J. Iber. Geol. 33, 221–236.

Bourquin, S., Guillocheau, F., Péron, S., 2009. Braided rivers within an arid alluvial plain (example from the lower triassic, western german basin): Recognition criteria and

expression of stratigraphic cycles. Sedimentology 56, 2235–2264. https://doi.org/10.1111/j.1365-3091.2009.01078.x

Bourquin, S., Peron, S., Durand, M., 2006. Lower Triassic sequence stratigraphy of the western part of the Germanic Basin (west of Black Forest): Fluvial system evolution through time and space. Sediment. Geol. 186, 187–211. https://doi.org/10.1016/j.sedgeo.2005.11.018

Bourquin, S., Rigollet, C., Bourges, P., 1998. High-resolution sequence stratigraphy of an alluvial fan-fan delta environment: Stratigraphic and geodynamic implications - An example from the Keuper Chaunoy Sandstones, Paris Basin. Sediment. Geol. 121, 207–237. https://doi.org/10.1016/S0037-0738(98)00081-5

Bridge, J.S., 2003. Rivers and Floodplains. Forms, Processes, and Sedimentary Record. Wiley-Blackwell.

Brookfield, M.E., Silvestro, M.E., 2010. Eolian systems, in: Walker, R.G., James, N.P. (Eds.), Facies Models. Geological Association of Canada, pp. 139–166.

Buatois, L.A., Mángano, M.G., 2004. Animal-substrate interactions in freshwater environments: Applications of ichnology in facies and sequence stratigraphic anlaysis of fluvio-lacustrine successions. Geol. Soc. Spec. Publ. 228, 311–333. https://doi.org/10.1144/GSL.SP.2004.228.01.14

Buatois, L.A., Netto, R.G., Gabriela Mángano, M., Carmona, N.B., 2013. Global deglaciation and the re-appearance of microbial matground-dominated ecosystems in the late Paleozoic of Gondwana. Geobiology 11, 307–317. https://doi.org/10.1111/gbi.12038

Burg, J.-P., Brunel, M., Gapais, D., Chen, G.M., Liu, G.H., 1984. Deformation of leucogranites of the cristalline main central thrust sheet in southern Tibet (China). J. Struct. Geol. 6, 535–542. https://doi.org/10.1016/0191-8141(84)90063-4

Burgess, S.D., Bowring, S., Shen, S. -z., 2014. High-precision timeline for Earth's most severe extinction. Proc. Natl. Acad. Sci. U. S. A. 111, 3316–3321. https://doi.org/10.1073/pnas.1317692111

Cain, S.A., Mountney, N.P., 2009. Spatial and temporal evolution of a terminal fluvial fan system: The permian organ rock formation, South-east Utah, USA. Sedimentology 56, 1774–1800. https://doi.org/10.1111/j.1365-3091.2009.01057.x

Caudill, M.R., Driese, S.G., Mora, C.I., 1996. Preservation of a paleo-vertisol and an estimate of Late Mississippian paleoprecipitation. J. Sediment. Res. 66, 58–70. https://doi.org/10.1306/D42682B1-2B2[illegible]-11D7-8648000102C1865D

Chamyal, L.S., Khadkikar, A.S., Malik, J.N., Maurya, D.M., 1997. Sedimentology of the Narmada alluvial fan, western India. Sediment. Geol. 107, 263–279. https://doi.org/10.1016/S0037-0738(96)00030-9

Charton, R., Bertotti, G., Arnould, A.D., Storms, J.E.A., Redfern, J., 2020. Low-temperature thermochronology as a control on vertical movements for semi-quantitative source-to-sink analysis: A case study for the Permian to Neogene of Morocco and surroundings. Basin Res. 33, 1337–1383.

Chu, D., Tong, J., Bottjer, D.J., Song, Haijun, Song, Huyue, Benton, M.J., Tian, L., Guo, W., 2017. Microbial mats in the terrestrial Lower Triassic of North China and implications for the Permian–Triassic mass extinction. Palaeogeogr. Palaeoclimatol. Palaeoecol. 474, 214–231. https://doi.org/10.1016/j.palaeo.2016.06.013

Chu, D., Tong, J., Song, H., Benton, M.J., Bottjer, D.J., Song, H., Tian, L., 2015. Early Triassic wrinkle structures on land: stressed environments and oases for life. Sci. Rep. 5, 1–8. https://doi.org/10.1038/srep10109

Clemmensen, L.B., Abrahamsen, K., 1983. Aeolian stratification and facies association in desert sediments, Arran basin (Permian), Scotland. Sedimentology 30, 311–339. https://doi.org/https://doi.org/10.1111/j.1365-3091.1983.tb00676.x

Cornée, J.-J., 1989. Le Haut-Atlas occidental paléozoïque: un relief de l'histoire hercynienne du Maroc occidental: stratigraphie, sédimentation et tectonique. Aix-Marseille 3.

Currie, B.S., 1997. Sequence stratigraphy of nonmarine Jurassic-Cretaceous rocks, central Cordilleran foreland-basin system. Geol. Soc. Am. Bull. 109, 1206–1222.

De Pachtère, P., 1983. Le volcanisme permien et fini-triasique dans le Haut-Atlas de Marrakech (Maroc): Approche pétrologique et géochimique. Grenoble.

Domènech, M., Stockli, D.F., Teixell, A., 2018. Detrital zircon U–Pb provenance and palaeogeography of Triassic rift basins in the Marrakech High Atlas. Terra Nov. 30, 310–318. https://doi.org/10.1111/ter.12340

Domènech, M., Teixell, A., Babault, J., Arboleya, M.-L., 2015. The inverted Triassic rift of the Marrakech High Atlas: A reappraisal of basin geometries and faulting histories. Tectonophysics 663, 177–191. https://doi.org/10.1016/j.tecto.2015.03.017

Duffaud, F., Brun, L., Plauchut, B., 1966. Le bassin du Sud-Ouest marocain. Bassins sédimentaires du litoral Africain 1, 5–26.

Durand, M., Bourquin, S., 2013. Criteria for the identification of ventifacts in the geological record: A review and new insights. Comptes Rendus Geosci. 345, 111–125. https://doi.org/10.1016/j.crte.2013.02.004

Eide, C.H., Suslova, A.A., Helland-hansen, W., 2018. Linking an Early Triassic delta to antecedent topography : Source-to-sink study of the southwestern Barents Sea margin. GSA Bull. 130, 263–283. https://doi.org/https://doi.org/10.1130/B31639.1

El Arabi, E.H., 1988. Le Permo-Trias du flanc sud du Haut Atlas de Marrakech. Sédimentologie, cartographie et paléogéographie. Grenoble.

El Arabi, E.H., Diez, J.B., Broutin, J., Essamoud, R., 2006a. Première caractérisation palynologique du Trias moyen dans le Haut Atlas ; implications pour l'initiation du rifting téthysien au Maroc. Comptes Rendus Geosci. 338, 641–649. https://doi.org/10.1016/J.CRTE.2006.04.001

El Arabi, E.H., Ferrandini, J., Essamoud, R., 2003. Triassic stratigraphy and structural evolution of a rift basin: the Es Çour basin, High atlas of Marrakech, Morocco. J. African Earth Sci. 36, 29–39. https://doi.org/10.1016/S0899-5362(03)00020-4

El Arabi, E.H., Hafid, M., Ferrandini, J., Essamoud, R., 2006b. Interprétation de la série syn-rift haut-atlasique en termes de séquences tectonostratigraphiques, transversale de Telouet, Haut Atlas (Maroc). Notes Mém. Serv. géol. Maroc 541, 93–101.

Ellouz, N., Patriat, M., Gaulier, J.-M.M., Bouatmani, R., Sabounji, S., 2003. From rifting to Alpine inversion: Mesozoic and Cenozoic subsidence history of some Moroccan basins. Sediment. Geol. 156, 185–212. https://doi.org/10.1016/S0037-0738(02)00288-9

Ernest, K.K., Kouadio, G.J.-M., Eric, D., Valérie, W.A., Jan, N., 2019. Analysis of Quaternary Sediments of Quartz Grains Applied to the Identification of the Environment of Some Ivory Beaches East of Abidjan (Côte d'Ivoire). Int. J. Environ. Clim. Chang. 486–502. https://doi.org/10.9734/ijecc/2019/v9i930134

Erwin, D.H., 1994. The Permo–Triassic extinction. Nature 367, 231–236. https://doi.org/10.1038/367231a0

Esteban, M., Klappa, C.F., 1983. Subaerial Exposure Environment, in: Scholle, P.A., Bebout, D.G., Moore, C.H. (Eds.), Carbonate Depositional Environments. American Association of Petroleum Geologists, pp. 2–54.

Ezquerro, L., Luzón, A., Simón, J.L., Liesa, C.L., 2019. Alluvial sedimentation and tectono-stratigraphic evolution in a narrow extensional zigzag basin margin (northern Teruel Basin, Spain). J. Palaeogeogr. 8, 1–25. https://doi.org/10.1186/s42501-019-0044-4

Fabuel-Perez, I., Redfern, J., Hodgetts, D., 2009. Sedimentology of an intra-montane rift-controlled fluvial dominated succession: The Upper Triassic Oukaimeden Sandstone Formation, Central High Atlas, Morocco. Sediment. Geol. 218, 103–140. https://doi.org/10.1016/j.sedgeo.2009.04.006

Fisher, J.A., Krapf, C.B.E., Lang, S.C., Nichols, G.J., Payenberg, T.H.D., 2008. Sedimentology and architecture of the Douglas Creek terminal splay, Lake Eyre, central Australia. Sedimentology 55, 1915–1930. https://doi.org/https://doi.org/10.1111/j.1365-3091.2008.00974.x

Fisher, J.A., Nichols, G.J., Waltham, D.A., 2007. Unconfined flow deposits in distal sectors of fluvial distributary systems: Examples from the Miocene Luna and Huesca Systems,

northern Spain. Sediment. Geol. 195, 55–73. https://doi.org/10.1016/j.sedgeo.2006.07.005

Frey, R.W., Pemberton, S.G., Fagerstrom, J.A., 1984. Morphological, ethological, and environmental significance of the ichnogenera Scoyenia and Ancorichnus. J. Paleontol. 58, 511–528.

Freytet, P., 1984. Les sédiments lacustres carbonatés et leurs transformations par émersion et pédogenèse. Importance de leur identification pour les reconstitutions paléogéographiques. Bull. des centres Rech. Explor. Elf Aquitaine 8, 223–246.

Frizon de Lamotte, D., Fourdan, B., Leleu, S., Leparmentier, F., De Clarens, P., 2015. Style of rifting and the stages of Pangea breakup. Tectonics 34, 1009–1029. https://doi.org/10.1002/2014TC003760

Frizon de Lamotte, D., Leturmy, P., Missenard, Y., Khomsi, S., Ruiz, G., Saddiqi, O., Guillocheau, F., Michard, A., 2009. Mesozoic and Cenozoic vertical movements in the Atlas system (Algeria, Morocco, Tunisia): an overview. Tectonophysics 475, 9–28. https://doi.org/10.1016/J.TECTO.2008.10.024

Galán-Abellán, B., López-Gómez, J., Barrenechea, J.F., Marzo, M., De la Horra, R., Arche, A., 2013. The beginning of the Buntsandstein cycle (Early-Middle Triassic) in the Catalan Ranges, NE Spain: Sedimentary and palaeogeographic implications. Sediment. Geol. 296, 86–102. https://doi.org/10.1016/j.sedgeo.2013.08.006

Galfetti, T., Hochuli, P.A., Brayard, A., Bucher, H., Weissert, H., Vigran, J.O., 2007. Smithian-Spathian boundary event: Evidence for global climatic change in the wake of the end-Permian biotic crisis. Geology 35, 291–294. https://doi.org/10.1130/G23117A.1

Gastaldo, R.A., Kus, K., Tabor, N., Neveling, J., 2020. Calcic vertisols in the upper daptocephalus assemblage zone, balfour formation, Karoo Basin, South Africa: Implications for late permian climate. J. Sediment. Res. 90, 609–628. https://doi.org/10.2110/JSR.2020.32

Geißler, V., 2006. Classification and geochemistry of arid and semi-arid paleosols. TU Bergakademie Freiberg.

Geluk, M.C., 2005. Stratigraphy and tectonics of Permo-Triassic basins in the Netherlands and surrounding areas. Thesis.

Geluk, M.C., Röhling, H.G., 1997. High-resolution sequence stratigraphy of the Lower Triassic "Buntsandstein" in the Netherlands and northwestern Germany. Geol. en Mijnb. 76, 227–246.

Ghazi, S., Mountney, N.P., 2009. Facies and architectural element analysis of a meandering fluvial succession: The Permian Warchha Sandstone, Salt Range, Pakistan. Sediment. Geol. 221, 99–126. https://doi.org/10.1016/j.sedgeo.2009.08.002

Gibert, J.M., Saez, A., 2009. Paleohydrological significance of trace fossil distribution in Oligocene fluvial-fan-to-lacustrine systems of the Ebro Basin, Spain. Palaeogeogr. Palaeoclimatol. Palaeoecol. 272, 162–175. https://doi.org/https://doi.org/10.1016/j.palaeo.2008.10.030

Goudemand, N., Romano, C., Leu, M., Bucher, H., Trotter, J.A., Williams, I.S., 2019. Dynamic interplay between climate and marine biodiversity upheavals during the early Triassic Smithian -Spathian biotic crisis. Earth-Science Rev. 195, 169–178. https://doi.org/10.1016/j.earscirev.2019.01.013

Gugliotta, M., Saito, Y., Ben, B., Sieng, S., Oliver, T.S.N., 2018. Sedimentology of late Holocene fluvial levee and point-bar deposits from the Cambodian tract of the Mekong river. J. Geol. Soc. London. 175, 176–186. https://doi.org/10.1144/jgs2017-047

Hasiotis, S.T., 1997. Redefining continental ichnology and the Scoyenia ichnofacies. University of Colorado, Boulder.

Jalil, N., Janvier, P., Steyer, J.-S., 2009. A new cyclotosaurid (Amphibia, Temnospondyli) from the Triassic of Argana Basin (High Atlas Mountains, Morocco); Biostratigraphic implications. First Int. Congr. North African Vertebr. Palaeontol. 36–37.

Jalil, N.-E., Dutuit, J.-M., 1996. Permian captorhinid reptiles from the Argana Formation, Morocco. Palaeontology 39, 907–918.

Jalil, N.-E., Janvier, P., 2005. Les pareiasaures (Amniota, Parareptilia) du Permien supérieur du Bassin d'Argana, Maroc. Geodiversitas 27, 35–132.

Jenny, J., 1983. Les décrochements de l'Atlas de Demnat (Haut Atlas central, Maroc): prolongation orientale de la zone décrochement du Tizi n'Test et clef de la compréhension de la tectonique atlasique. Eclogae Geol. Helv. 76, 243–251.

Jenny, J., Izart, A., Lesage, J.L., 1989. La boutonnière d'Aït Tamlil: évolution tectono-sédimentaire durant le viséen et structuration du segment hecynien du Haut-Atlas central (Maroc). Notes Mémoires Serv. Géologique Maroc 335, 239–250.

Jorgensen, P.J., Fielding, C.R., 1996. Facies architecture of alluvial floodbasin deposits: Three-dimensional data from the UpperTriassic Callide Coal Measures of east-central Queensland, Australia. Sedimentology 43, 479–495. https://doi.org/10.1046/j.1365-3091.1996.d01-25.x

Klein, H., Voigt, S., Hminna, A., Saber, H., Schneider, J.W., Hmich, D., 2010. Early Triassic archosaur-dominated footprint assemblage from the Argana Basin (western High Atlas, Morocco). Ichnosan Int. J. Plant Anim. 17, 215–227. https://doi.org/10.1080/10420940.2010.510030

Klein, H., Voigt, S., Saber, H., Schneider, J.W., Hminna, A., Fischer, J., Lagnaoui, A., Brosig, A., 2011. First occurrence of a Middle Triassic tetrapod ichnofauna from the Argana Basin (western High Atlas, Morocco). Palaeogeogr. Palaeoclimatol. Palaeoecol. 307, 218–231. https://doi.org/:10.1016/j.palaeo.2011.05.021

Kraus, M.J., 1999. Paleosols in clastic sedimentary rocks: Their geologic applications. Earth Sci. Rev. 47, 41–70. https://doi.org/10.1016/S0012-8252(99)00026-4

Kraus, M.J., Aslan, A., 1993. Eocene hydromorphic Paleosols; significance for interpreting ancient floodplain processes. J. Sediment. Res. 63, 453–463. https://doi.org/https://doi.org/10.1306/D4267B22-2B26-11D7-8648000102C1865D

Laville, E., 1980. Tectonique et microtectonique d'une partie du versant sud Haut Atlas marocain (boutonnière de Skoura-Toundout). Notes Mémoires Serv. Géologique Maroc 41, 1–183.

Laville, E., Petit, J.-P., 1984. Role of synsedimentary strike-slip faults in the formation of Moroccan Triassic basins. Geology 12, 424–427.

Laville, E., Piqué, A., 1991. La Distension crustale atlantique et atlasique au Maroc au début du Mésozoïque; le rejeu des structures hercyniennes. Bull. la Société géologique Fr. 162, 1161–1171.

Laville, E., Piqué, A., Amrhar, M., Charroud, M., 2004. A restatement of the Mesozoic Atlasic rifting (Morocco). J. African Earth Sci. 38, 145–153.

Le Roy, P., Piqué, A., 2001. Triassic-Liassic western Moroccan synrift basins in relation to the Central Atlantic opening. Mar. Geol. 172, 359–381. https://doi.org/10.1016/S0025-3227(00)00130-4

Leleu, S., Hartley, A.J., van Oosterhout, C., Kennan, L., Ruckwied, K., Gerdes, K., 2016. Structural, stratigraphic and sedimentological characterisation of a wide rift system: The Triassic rift system of the Central Atlantic Domain. Earth-Science Rev. 158, 89–124. https://doi.org/https://doi.org/10.1016/j.earscirev.2016.03.008

Linol, B., Bercovici, A., Bourquin, S., Diez, J.B., Lopez-Gómez, J., Broutin, J., Durand, M., Villanueva-Amadoz, U., 2009. Late Permian to Middle Triassic correlations and palaeogeographical reconstructions in south-western European basins: New sedimentological data from Minorca (Balearic Islands, Spain). Sediment. Geol. 220, 77–94. https://doi.org/10.1016/j.sedgeo.2009.06.003

Lloret, J., López-Gómez, J., Heredia, N., Martín-González, F., de la Horra, R., Borruel-Abadía, V., Rodrigo, A., Barrenechea, J.F., García-Sansegundo, J., Galé, C., Ubide, T., Gretter, N., Diez, J.B., Juncal, M., Lago, M., 2021. Transition between Variscan and Alpine cycles in the Pyrenean-Cantabrian Mountains (N Spain): Geodynamic evolution of near-equator European Permian basins. Glob. Planet. Change 207, 1–25. https://doi.org/10.1016/j.gloplacha.2021.103677

Lorentz, V., Nicholls, I.A., 1976. The Permo-Carboniferous Basin and Range province of Europe. An application of plate tectonics, in: Falke, H. (Ed.), The Continental Permian in Central, West, and South Europe. Reidel Publishing Company, Dordrecht, pp. 313–342.

Machette, N., 1985. Calcic soils of southwestern United States, in: Weide, D.L. (Ed.), Soils and Quaternary Geology of the Southwestern United States. Geological Society of America, pp. 1–21. https://doi.org/https://doi.org/10.1130/SPE203-p1

Mack, G.H., James, W.C., Monger, H.C., 1993. Classification of paleosols. Geol. Soc. Am. Bull. 105, 129–136.

Mader, N.K., Redfern, J., 2011. A sedimentological model for the continental upper triassic tadrart ouadou sandstone member: Recording an interplay of climate and tectonics (Argana valley; south-west Morocco). Sedimentology 58, 1247–1282. https://doi.org/10.1111/j.1365-3091.2010.01204.x

Makhlouf, I.M., Amireh, B.S., Abed, A.M., 2010. Sedimentology and morphology of Quaternary alluvial fans in Wadi Araba, Jordan. Jordan J. Earth Environ. Sci. 3, 79–98.

Manspeizer, W., 1988. Triassic–Jurassic rifting and opening of the Atlantic: an overview. Dev. Geotecton. 22, 41–79.

Manspeizer, W., Puffer, J.H., Cousminer, H.L., 1978. Separation of Morocco and eastern North America: a Triassic-Liassic stratigraphic record. Geol. Soc. Am. Bull. 89, 901–920.

Marriott, S.B., Wright, V.P., 2004. Mudrock deposition in an ancient dryland system: Moor Cliffs Formation, Lower Old Red Sandstone, southwest Wales, UK. Geol. J. 39, 277–298. https://doi.org/10.1002/gj.990.

Marriott, S.B., Wright, V.P., 2006. Investigating paleosol completeness and preservation in mid-Paleozoic alluvial paleosols: A case study in paleosol taphonomy from the Lower

Old Red Sandstone. Spec. Pap. Geol. Soc. Am. 416, 43–52. https://doi.org/10.1130/2006.2416(03)

Marriott, S.B., Wright, V.P., Williams, B.P.J., 2005. A new evaluation of fining upward sequences in a mud-rock dominated succession of the Lower Old Red Sandstone of South Wales, UK. Spec. Publ. Int. Assoc. Sedimentol. 35, 517–529.

Marzoli, A., Bertrand, H., Knight, K.B., Cirilli, S., Buratti, N., Vérati, C., Nomade, S., Renne, P.R., Youbi, N., Martini, R., 2004. Synchrony of the Central Atlantic magmatic province and the Triassic-Jurassic boundary climatic and biotic crisis. Geology 32, 973–976. https://doi.org/10.1130/G20652.1

Mather, A.E., Hartley, A., 2005. Flow events on a hyper-arid alluvial fan: Quebrada Tambores, Salar de Atacama, northern Chile. Geol. Soc. Spec. Publ. 251, 9–24. https://doi.org/10.1144/GSL.SP.2005.251.01.02

Mattis, A.F., 1977. Nonmarine Triassic sedimentation, Central High Atlas Mountains, Morocco. J. Sediment. Res. 47, 107–119.

McKie, T., Shannon, P.M., 2011. Comment on "The Permian–Triassic transition and the onset of Mesozoic sedimentation at the northwestern peri Tethyan domain scale: Palaeogeographic maps and geodynamic implications" by S. Bourquin, A. Bercovici, J. López-Gómez, J. B. Diez, J. Broutin, A. . Palaeogeogr. Palaeoclimatol. Palaeoecol. 299, 265–280.

Medici, G., Boulesteix, K., Mountney, N.P., West, L.J., Odling, N.E., 2015. Palaeoenvironment of braided fluvial systems in different tectonic realms of the Triassic Sherwood Sandstone Group, UK. Sediment. Geol. 329, 188–210. https://doi.org/10.1016/j.sedgeo.2015.09.012

Medina, F., 1994. Evolution structurale du Haut Atlas occidental et des régions voisines du Trias à l'actuel, dans le cadre de l'ouverture de l'atlantique central et de la collision Afrique-Europe. Mohamed V, Rabat.

Medina, F., Vachard, D., Colin, J.-P., Ouarhache, D., Ahmamou, M., 2001. Charophytes et ostracodes du niveau carbonaté de Taourirt Imzilen (Membre d'Aglegal, Trias d'Argana); implications stratigraphiques. Bull. Inst. Sci. Rabat 23, 21–26.

Mees, F., Carmen, C., Juan, H., Eric Van Ranst, 2012. The nature and significance of variations in gypsum crystal morphology in dry lake basins. J. Sediment. Res. 82, 41–56. https://doi.org/10.2110/jsr.2012.3

Meijer, H.J.M., 2007. Erwin, DG 2006. Extinction. How life on earth nearly ended 250 million years ago.–Princeton, New Jersey, Princeton University Press. PalArch's J. Vertebr. Palaeontol. 4, 1.

Ménard, G., Molnar, P., 1988. Collapse of a Hercynian Tibetan Plateau into a late Palaeozoic European Basin and Range province. Nature 334, 235–237.

Méndez-Bedia, I., Gallastegui, G., Busquets, P., Césari, S.N., Limarino, C.O., Prats, E., Cardó, R., Colombo, F., 2020. Pedogenic and subaerial exposure microfabrics in a late Carboniferous-early Permian carbonate-volcanic lacustrine-palustrine system (San Ignacio Formation, Frontal Cordillera, Argentina). Andean Geol. 47, 275–294. https://doi.org/10.5027/andgeoV47n2-3214

Miall, A.D., 1977. A review of the braided river depositional environment. Earth-Science Rev. 13, 1–62.

Miall, A.D., 1978. Lithofacies types and vertical profile models in braided river deposits: a summary. In: Miall, A.D. (Ed.), Fluvial Sedimentology. Can. Soc. Pet. Geol. Mem. 5, 597–604.

Miall, A.D., 1996. The Geology of Fluvial Deposits.

Milroy, P.G., Wright, V.P., 2000. A highstand oolitic sequence and associated facies from a Late Triassic lake basin, south-west England. Sedimentology 47, 187–209. https://doi.org/https://doi.org/10.1046/j.1365-3091.2000.00282.x

Milroy, P.G., Wright, V.P., 2002. Fabrics, facies control and diagenesis of lacustrine ooids and associated grains from the Upper Triassic, southwest England. Geol. J. 37, 35–53. https://doi.org/10.1002/gj.901

Missenard, Y., Taki, Z., de Lamotte, D.F., Benammi, M., Hafid, M., Leturmy, P., Sébrier, M., 2007. Tectonic styles in the Marrakesh High Atlas (Morocco): The role of heritage and mechanical stratigraphy. J. African Earth Sci. 48, 247–266.

Moragas, M., Vergés, J., Nalpas, T., Saura, E., Martín-Martín, J.D., Messager, G., William Hunt, D., 2017. The impact of syn- and post-extension prograding sedimentation on the development of salt-related rift basins and their inversion : Clues from analogue modelling. Mar. Pet. Geol. 88, 985–1003. https://doi.org/10.1016/j.marpetgeo.2017.10.001

Mukhopadhyay, A., Mazumdar, P., van Loon, A.J. (Tom., 2016. A new 'superassemblage' model explaining proximal-to-distal and lateral facies changes in fluvial environments, based on the Proterozoic Sanjauli Formation (Lesser Himalaya, India). J. Palaeogeogr. 5, 391–408. https://doi.org/10.1016/j.jop.2016.08.001

Muravchik, M., Bilmes, A., D'Elia, L., Franzese, J.R., 2014. Alluvial fan deposition along a rift depocentre border from the Neuquén Basin, Argentina. Sediment. Geol. 301, 70–89. https://doi.org/10.1016/j.sedgeo.2013.12.007

Nanson, G.C., Croke, J.C., 1992. A genetic classification of floodplains. Geomorphology 4, 459–486. https://doi.org/10.2113/gsecongeo.3.7.611

Nichols, G.J., Fisher, J.A., 2007. Processes, facies and architecture of fluvial distributary system deposits. Sediment. Geol. 195, 75–90.

Oliva-Urcia, B., Casas, A.M., Moussaid, B., Villalaín, J.J., El Ouardi, H., Soto, R., Torres-López, S., Román-Berdiel, T., 2016. Tectonic fabrics vs. mineralogical artifacts in AMS analysis: A case study of the Western Morocco extensional Triassic basins. J. Geodyn. 94, 13–33.

Olsen, P.E., Kent, D.V., Et-Touhami, M., 2003. Chronology and stratigraphy of the Fundy and related Nova Scotia offshore basins and Morocco based on core and outcrop. Conventional Core Workshop. Halifax, Geological Society of America (NE Section) and Atlantic Geoscience Society.

Olsen, T., 1995. Sequence stratigraphy, alluvial architecture and potential reservoir heterogeneities of fluvial deposits: evidence from outcrop studies in Price Canyon, Utah (Upper Cretaceous and Lower Tertiary), in: Sequence Stratigraphy on the Northwest European Margin. Norw. Petrol. Soc. Spec. Publ., pp. 75–96.

Ouanaimi, H., 1989. Evolution sédimentaire et tectonique de la partie orientale du massif ancien du Haut-Atlas (Maroc). Université Sciences et Techniques du Languedoc, Montpellier.

Ouanaimi, H., Petit, J.P., 1992. La limite sud de la chaîne hercynienne dans le Haut Atlas (Maroc): reconstitution d'un saillant non déformé. Bull. la Société géologique Fr. 163, 63–72.

Palermo, D., Aigner, T., Geluk, M., Poeppelreiter, M., Pipping, K., 2008. Reservoir potential of a lacustrine mixed carbonate/siliciclastic gas reservoir: The Lower Triassic Rogenstein in the Netherlands. J. Pet. Geol. 31, 61.

Paul, J., Peryt, T.M., Burne, R. V., 2011. Kalkowsky's Stromatolites and Oolites (Lower Buntsandstein, Northern Germany). Lect. Notes Earth Sci. 131, 187–205. https://doi.org/10.1007/978-3-642-10415-2

Payne, J.L., Lehrmann, D.J., Wei, J., Orchard, M.J., Schrag, D.P., Knoll, A.H., 2004. Large perturbations of the carbon cycle during recovery from the end-Permian extinction. Science (80-.). 305, 506–509.

Perez, N.D., Teixell, A., Gómez-Gras, D., Stockli, D.F., 2019. Reconstructing Extensional Basin Architecture and Provenance in the Marrakech High Atlas of Morocco: Implications for Rift Basins and Inversion Tectonics. Tectonics 38, 1584–1608. https://doi.org/10.1029/2018TC005413

Péron, S., Bourquin, S., Fluteau, F., Guillocheau, F., 2005. Paleoenvironment reconstructions and climate simulations of the Early Triassic: impact of the water and sediment supply on the preservation of fluvial systems. Geodin. Acta 18, 431–446. https://doi.org/10.3166/ga.18.431-446

Petit, J., Beauchamp, J., 1986. Synsedimentary faulting and palaeocurrent patterns in the Triassic sandstones of the High Atlas (Morocco). Sedimentology 33, 817–829.

Proust, F., Petit, J.-P., Tapponnier, P., 1977. L'accident du Tizi n'Test et le rôle des décrochements dans la tectonique du Haut Atlas occidental (Maroc). Bull. la Société géologique Fr. 7, 541–551.

Ravidà, D.C.G., Caracciolo, L., Henares, S., Janßen, M., Stollhofen, H., 2022. Drainage and environmental evolution across the Permo–Triassic boundary in the south-east Germanic Basin (north-east Bavaria). Sedimentology 69, 501–536. https://doi.org/10.1111/sed.12913

Redfern, J., Shannon, P.M., Williams, B.P.J., Tyrrell, S., Joleu, S., Fabuel Perez, I., Baudon, C., Štolfová, K., Hodgetts, D., Van Lanen, X., Spekkijder, A., Haughton, P.D.W., Daly, J.S., 2010. An integrated study of Permo-Triassic basins along the North Atlantic passive margin: Implication for future exploration. Pet. Geol. Conf. Proc. 7, 921–936. https://doi.org/10.1144/0070921

Rees, P.M., 2002. Land-plant diversity and the end-Permian mass extinction. Geology 30, 827–830.

Retallack, G.J., 1988. Field recognition of paleosols., in: Reinhardt, J., Sigleo, W.R. (Eds.), Paleosols and Weathering Through Geologic Time: Principles and Applications. Geol. Soc. Am. Spec. Paper, pp. 1–20.

Retallack, G.J., 1997. A color guide to paleosols.

Retallack, G.J., 2001. Soils of the past: An Introduction to Paleopedology. Oxford: Blackwell Science.

Romano, C., Goudemand, N., Vennemann, T.W., Ware, D., Schneebeli-Hermann, E., Hochuli, P.A., Brühwiler, T., Brinkmann, W., Bucher, H., 2013. Climatic and biotic

upheavals following the end-Permian mass extinction. Nat. Geosci. 6, 57–60. https://doi.org/10.1038/ngeo1667

Saber, H., El Wartiti, M., Hmich, D., Schneider, J.W., 2007. Tectonic evolution from the Hercynian shortening to the Triassic extension in the Paleozoic sediments of the Western High Atlas (Morocco). J. Iber. Geol. 33, 31–40.

Schieber, J., Bose, P.K., Eriksson, P.G., Banerjee, S., Sarkar, S., Alterman, W., Catuneanu, O., 2007. Atlas of microbial mat features preserved within the siliciclastic rock record, Atlases in Geosciences 2. Elsevier.

Schneider, J.W., Körner, F., Roscher, M., Kroner, U., 2006. Permian climate development in the northern peri-Tethys area — The Lodève basin, French Massif Central, compared in a European and global context. Palaeogeogr. Palaeoclimatol. Palaeoecol. 240, 161–183. https://doi.org/10.1016/j.palaeo.2006.03.057

Schneider, J.W., Lucas, S.G., Scholze, F., Voigt, S., Marchetti, L., Klein, H., Opluštil, S., Werneburg, R., Golubev, V.K., Barrick, J.E., Nemyrovska, T., Ronchi, A., Day, M.O., Silantiev, V. V., Rößler, R., Saber, H., Linnemann, U., Zharinova, V., Shen, S.Z., 2020. Late Paleozoic–early Mesozoic continental biostratigraphy — Links to the Standard Global Chronostratigraphic Scale. Palaeoworld 29, 186–238. https://doi.org/10.1016/J.PALWOR.2019.09.001

Scholze, F., Hamad, A.A., Schneider, J.W., Golubev, K., Sennikov, A.G., Voigt, S., Uhl, D., 2017. An enigmatic “conchostracan” fauna in the eastern Dead Sea Region of Jordan: First records of Rossolimnadiopsis Novozhilov from the Early Triassic Ma’in Formation. Palaeogeogr. Palaeoclimatol. Palaeoecol. 466, 314–325. https://doi.org/10.1016/j.palaeo.2016.11.047

Sheldon, N.D., Tabor, N.J., 2009. Quantitative paleoenvironmental and paleoclimatic reconstruction using paleosols. Earth Sci. Rev. 95, 1–52. https://doi.org/10.1016/j.earscirev.2009.03.004

Shen, J., Chen, J., Yu, J., Algeo, T.J., Smith, R.M.H., Botha, J., Frank, T.D., Fielding, C.R., Ward, P.D., Mather, T.A., 2023. Mercury evidence from southern Pangea terrestrial sections for end-Permian global volcanic effects. Nat. Commun. 14, 1–9.

Smith, R., Kitching, J., 1997. Sedimentology and vertebrate taphonomy of the Tritylodon Acme Zone: A reworked palaeosol in the Lower Jurassic Elliot formation, karoo supergroup, South Africa. Palaeogeogr. Palaeoclimatol. Palaeoecol. 131, 29–50. https://doi.org/10.1016/S0031-0182(96)00143-5

Smith, R.M.H., 1993. Vertebrate Taphonomy of Late Permian Floodplain Deposits in the Southwestern Karoo Basin of South Africa. Palaios 8, 45–67. https://doi.org/10.2307/3515221

Sohn, Y.K., Rhee, C.W., Kim, B.C., 1999. Debris flow and hyperconcentrated flood-flow deposits in an alluvial fan, northwestern part of the Cretaceous Yongdong Basin, Central Korea. J. Geol. 107, 111–132. https://doi.org/10.1086/314334

Soil Survey Staff, 1975. Soil Taxonomy: A basic system of soil classification for making and interpreting soil surveys. US Department of Agriculture Handbook 436.

Soil Survey Staff, 2022. Keys to Soil Taxonomy, 13th ed. USDA-Natural Resources Conservation Service.

Spalletti, L.A., Limarino, C.O., Colombo Pino, F., 2010. Internal anatomy of an erg sequence from the Aeolian-fluvial system of the De La Cuesta Formation (Paganzo Basin, northwestern Argentina). Geol. Acta 8, 431–447. https://doi.org/10.1344/105.000001581

Stets, J., Wurster, P., 1982. Atlas and Atlantic-Structural Relations, in: Von Rad, U., Hinz, K., Sarnthein, M., Seibold, E. (Eds.), Geology of the Northwest African Continental Margin. Springer, pp. 69–85.

Sun, Y., Joachimski, M.M., Wignall, P.B., Yan, C., Chen, Y., Jiang, H., Wang, L., Lai, X., 2012. Lethally Hot Temperatures During the Early Triassic Greenhouse. Science (80-.). 338, 366–370. https://doi.org/10.1126/science.1224126

Szurlies, M., 2004. Magnetostratigraphy: The key to a global correlation of the classic Germanic Trias-case study Volpriehausen Formation (Middle Buntsandstein), Central Germany. Earth Planet. Sci. Lett. 227, 395–410. https://doi.org/10.1016/j.epsl.2004.09.011

Szurlies, M., 2007. Latest Permian to Middle Triassic cyclo-magnetostratigraphy from the Central European Basin, Germany: Implications for the geomagnetic polarity timescale. Earth Planet. Sci. Lett. 261, 602–619. https://doi.org/10.1016/j.epsl.2007.07.018

Tabor, N.J., Montañez, I.P., 2004. Morphology and distribution of fossil soils in the Permo-Pennsylvanian Wichita and Bowie Groups, north-central Texas, USA: implications for western equatorial Pangean palaeoclimate during icehouse-greenhouse transition. Sedimentology 51, 851–884. https://doi.org/10.1111/j.1365-3091.2004.00655.x

Tabor, N.J., Montañez, I.P., Kelso, K.A., Currie, B., Shipman, T., Colombi, C., 2006. A Late Triassic soil catena: Landscape and climate controls on paleosol morphology and

chemistry across the Carnian-age Ischigualasto-Villa Union basin, northwestern Argentina. Geol. Soc. Am. Spec. Pap. 416, 17–41. https://doi.org/10.1130/2006.2416(02).

Tabor, N.J., Sidor, C.A., Smith, R.M.H., Nesbitt, S.J., Angielczyk, K.D., 2017. Paleosols of the Permian-Triassic: proxies for rainfall, climate change and major changes in terrestrial tetrapod diversity. J. Vertebr. Paleontol. 37, 240–253. https://doi.org/https://doi.org/10.1080/02724634.2017.1415211

Tixeront, M., 1973. Lithostratigraphie et minéralisations cuprifères et uranifères stratiformes, syngénétiques et familières des formations détritiques permo-triasiques du couloir d'Argana, Haut Atlas occidental (Maroc). Not. Serv. Géol. Maroc 249, 147–177.

Tixeront, M., 1974. Carte géologique et minéralisations du couloir d'Argana au 1/100 000. Notes Mém. Serv. géol. Maroc 205.

Tooth, S., 2000. Process, form and change in dryland rivers: A review of recent research. Earth Sci. Rev. 51, 67–107. https://doi.org/10.1016/S0012-8252(00)00014-3

Tooth, S., 2005. Splay formation along the lower reaches of ephemeral rivers on the northern plains of arid central Australia. J. Sediment. Res. 75, 636–649. https://doi.org/10.2110/jsr.2005.052

Tourani, A., Benaouiss, N., Gand, G., Bourquin, S., Jalil, N.-E., Broutin, J., Battail, B., Germain, D., Khaldoune, F., Sebban, S., Steyer, J.S., Vacant, R., 2010. Evidence of an Early Triassic age (Olenekian) in Argana Basin (High Atlas, Morocco) based on new chirotherioid traces. Comptes Rendus - Palevol 9, 201–208. https://doi.org/10.1016/j.crpv.2010.05.001

Tourani, A., Lund, J.J., Benaouiss, N., Gaupp, R., 2000. Stratigraphy of Triassic syn-rift deposition in Western Morocco. Zentralblatt für Geol. und Paläontologie 9, 1193–1215.

Van Houten, F.B., 1977. Triassic-Liassic deposits of Morocco and East North America: A comparison. Bull. Am. Assoc. Pet. Geol. 61, 79–99.

van Toorenenburg, K.A., Donselaar, M.E., Noordijk, N.A., Weltje, G.J., 2016. On the origin of crevasse-splay amalgamation in the Huesca fluvial fan (Ebro Basin, Spain): Implications for connectivity in low net-to-gross fluvial deposits. Sediment. Geol. 343, 156–164. https://doi.org/10.1016/j.sedgeo.2016.08.008

Viseras, C., Soria, J.M., Durán, J.J., Pla, S., Garrido, G., García-García, F., Arribas, A., 2006. A large-mammal site in a meandering fluvial context (Fonelas P-1, Late Pliocene, Guadix Basin, Spain). Sedimentological keys for its paleoenvironmental reconstruction. Palaeogeogr. Palaeoclimatol. Palaeoecol. 242, 139–168. https://doi.org/10.1016/j.palaeo.2006.05.013

Vogel, E., Missotten, R., Desuter, F., 1980. Carte géologique du Maroc au 1/100 000e feuille Oukaïmeden-Toubkal.

Voigt, T., Gaupp, R., Rolling, H.-G., 2011. Lake deposits of the Early Triassic Buntsandstein in Central Germany: Type localities of oolites and stromatolites, in: Proceedings of the 5th International Limnogeological Congress ILIC. pp. 191–211.

Wright, V.P., Marriott, S.B., 1996. A quantitative approach to soil occurrence in alluvial deposits and its application to the Old Red Sandstone of Britain. J. Geol. Soc. London. 153, 907–913. https://doi.org/10.1144/gsjgs.153.6.0907

Wright, V.P., Tucker, M.E., 1991. Calcretes: An introduction, Blackwell,. ed, The International Association of Sedimentologists.

Ziegler, P.A., Dèzes, P., 2006. Crustal evolution of Western and Central Europe. Geol. Soc. Mem. 32, 43–56. https://doi.org/10.1144/GSL.MEM.2006.032.01.03

Figure captions

Figure 1: Location of the study areas. (A) Triassic outcrops throughout the High Atlas mountain range: WHA = Western High Atlas, MHA = Marrakech High Atlas, CHA = Central High Atlas, EHA = Eastern High Atlas and MA = Middle High Atlas (Modified after Beauchamp, 1988; Laville and Piqué, 1991). (B) The areas in pink indicate Permian and Triassic outcrops. The white colour covers the Palaeozoic and post-Triassic outcrops (Benaouiss et al., 1996). Arrows indicate the location of the three sections (Irerhi in Argana Basin, Tanoumri and Aït Tamlil in MHA Basin). (C) Generalized lithostratigraphic column of the Argana Basin (t1 to t8 Units) and the Marrakech High Atlas basins (F1 to F6 Fm). The studied interval is from the uppermost part of the t2 and F2 units to the lowermost part of the t4 and F4 units, respectively. The numbers 1 to 15 refer to the dating levels: (1) Jalil and Dutuit (1996), Jalil and Janvier (2005); vertebrate remains, late Permian; (2) Tourani et al., (2010); tetrapod footprints, Olenekian (Early Triassic); (3) Klein et al., (2010), tetrapod footprints, Olenekian (Early Triassic); (4) Jalil et al., (2009), vertebrate remains, Middle Triassic; (5) Klein et al., (2011), tetrapod footprints, Middle Triassic; (6) Medina et al., (2001), charophytes and ostracods, Anisian (Middle Triassic); (7) Jalil (1999), vertebrate remains, Carnian (Late Triassic); (8) Jalil (1999) and Khaldoune et al., (2017), vertebrate remains, Carnian (Late Triassic); (9) Weems and Lucas (2015), conchostracan, uppermost Norian (Late Triassic); (10) Blackburn et al., (2013), zircon geochronology, end-Triassic; (11) Van Houten (1977), radiometric dating, Permian (Lower Permian); (12) Perez et al., (2019),

zircon geochronology, late Permian; (13) El Arabi et al., (2006), pollens, Middle Triassic (Middle Anisian); (14) Biron and Courtinat (1982), pollens, Late Triassic (Middle Carnian); (15) Cousminer and Manspeizer (1976), pollens, Late Triassic (Middle Carnian) and (16) Marzoli et al., (2004), radiometric dating, Lower Jurassic.

Figure 2: Sedimentological log, palaeosols, palaeocurrents, depositional environments, stratigraphic cycles and climate conditions of the Irerhi section in the Argana Basin. See Tables 1 to 3 for the facies, palaeosol, and environment codes and their description.

Figure 3: Irerhi area to the north of Argana village. (A) Geological map around the Irerhi section. (B) Details of the SB1 unconformity. (C) Details of the SB2 unconformity, highlighted by a white surface (Pg soil, see Table 2). See Figure 2 for the stratigraphic position of the unconformities.

Figure 4: Representative examples of facies and facies association types encountered in the late Permian to Early Triassic series, in the Argana and MHA basins. (A) Subunits, Braided River (RB) and SB2 unconformity in the Irerhi section. (B) and (C) respectively zooms of proximal alluvial fan (AFp) and med-alluvial fan (AFm1). (D) SB2 unconformity between t4a and t4b subunits, underlined by white hydromorphic soil (Pg). (E) Distal alluvial fan (AFp) characterizing t4a Subunit. (F) to (R) Tanoumri section in MHA basins. (F) SB1 unconformity between the late Permian (F2 Unit) and Early Triassic (F3 Unit). (G) to (I) late Permian palustrine deposit (PA) in the F2 Unit, composed of the C/C facies with stacked laminated carbonate (1) and brecciated claystone (2). (J) Lowermost part of the F3a Subunit, showing SB1 unconformity, palaeoreg deposit (RE) and proximal alluvial fan deposits (AFp). (K) Ventifacts from the base of F3a and t3a subunits, bars represent 1 cm. (L) and (M) illustrate the main facies of the med-alluvial fan deposits (AFm1). (N) Representative facies types from the distal alluvial fan (AFd) of the F3b Subunit. (O) Palustrine deposits (PA)

overlying by the distal alluvial fan (AFd) of the F3b Subunit; (P) Zoom of the gleyed mudstone, indicating the hydromorphic soil-gleying (Pg), see (O) for location; (Q) Close up view of the Cpa facies with various types of desiccation and root cracks which lead to intraclasts of brecciated facies, see (O) for location; (R) Pedogenic carbonates (Cpe) in the F3b Subunit, palaeosols (Pc-IV/Pc-VI) with prismatic carbonate nodules (P) horizon, hard and deformed carbonate horizons. See Tables 1, 2 and 3 for the meaning of the codes, the blue hammer is 28 cm length, the brown one is 33 cm length, and the stick is 1 m length.

Figure 5: (A) Geological map of the Permian and Triassic outcrops in the Marrakech High Atlas MHA (redrawn from Biron 1982) with the location of the Tanoumri section (white star). (B) Picture showing the details of the angular unconformity between the F2 (late Permian) and F3 (Lower Triassic) units. (C) Picture showing the details of the angular unconformity (SB2, yellow lines) between the Lower Triassic F4a Subunit and early Middle Triassic F4b Subunit in the Tanoumri section, white lines represent stratification. (D) Geological map of the Aït Tamlil area, Permian and Triassic outcrops (age code pt, i.e., purple and yellow color). (E) Zoom view of synthetic geological map around the studied zone and the location of the Aït Tamlil section (white star). (F) The Aït Tamlil outcrop view showing the unconformities between the late Permian F2 Unit and Lower Triassic F3 Unit (SB1) and between the F4a/F4b Middle Triassic subunits (SB2). See Figure 1B for the location of Tanoumri and Aït Tamlil sections.

Figure 6: Sedimentological log, palaeosols, palaeocurrents, depositional environments, stratigraphic cycles and climate conditions of the Tanoumri section in the Marrakech High Atlas basins (MHA). See Tables 1 to 3 for the facies, palaeosol and environment codes and their description. See Fig. 2 for legend.

Figure 7: Aeolian facies in the Tanoumri section, (A) aeolian dunes and sandsheet, the white arrows indicate the boundary surfaces, (B) zoom view of the area in the black box in (A), (C) and (D) grouped aeolian dunes, the cross-section is slightly perpendicular to oblique to the direction of the current in (C), and parallel to the direction of the current in (D).

Figure 8: Common types of facies and facies association in the Tanoumri and Aït Tamlil sections within MHA basins, from the Early Triassic to early Middle Triassic. Tanoumri section: (A) Pedogenic carbonate (Cpe) in the F3b Subunit, white arrows indicate the laminated carbonate, black arrow shows the alveolar septal structure associated to vertical desiccation (red arrow); (B) Zoom of Sq facies, well sorted and sub-to rounded quartz, associated to the brecciated facies of the Fig. 4Q; (C) The middle and upper part of the F3b Subunit, display the berm deposits (Bm) with wedge-planar foresets (Gh, Sl facies) of more sandy beds (D, black arrows indicate the continuous calcite coating particles) and pebbly beds (E, black arrows indicate calcite cement). (F) close up view of interstratified algal mats (AM); (G) Distal fluvial fan distributary system (FF), showing a flat sheet bed of the F4a Subunit; (H) Zoom showing Sb2 cylindrical burrow (Taenidium Barretti). Aït Tamlil section: (I) Different units and subunits of the Aït Tamlil section. (J) Zoom of the stacked Pc-IV calcretes in the lower part of the F3b Subunit; in med-alluvial fan (AFm1/AFm2), see location in (I). (K) Distal alluvial fan (AFd) deposits overlaying by lacustrine facies associations (L1/L2) of the F3b Subunit, see location in (I) and see details in L to N; (L) and (M) Lacustrine deposits (L1), respectively the oolitic shoal with COl and COr facies; (N) White arrows indicate the associated algal mats to COl or COr facies; (O) Oolitic sandstone lobes (L2), the black arrows point to glistening quartz grains, the blue arrows show ooliths in a sandy facies; (P) Lacustrine deposits (L3) of the F4a Subunit, separated from the F4b Subunit by the SB2 unconformity; (Q) Meandering river (RM) and floodplain (FP) deposits of the F4b Subunit.

The Fsm facies is associated to Pv soils with carbonate nodules and slickensides (white arrows). See Tables 1, 2 and 3 for the meaning of the codes.

Figure 9: Sedimentological column, palaeosols, palaeocurrents, depositional environments, stratigraphic cycles and climate conditions of the Aït Tamlil section in the Marrakech High Atlas basins. See Tables 1 to 3 for the facies, palaeosol and environment codes and their description. See Fig. 2 for legend.

Figure 10: Stratigraphic correlation of the late Permian - Lower Triassic - early Middle Triassic deposits showing sedimentary architectures, depositional environments and climate conditions within (1) Irerhi section in Argana Basin, (2) Tanoumri and (3) Aït Tamlil sections in Marrakech High Atlas (MHA) basins. See the location of the sedimentological sections in Figure 1B.

Figure 11: Palaeogeography of the Marrakech High Atlas basins during the Lower Triassic (especially F3a and F3b subunits). (A) Location of the MHA sections on the geological map. (B to E) Palaeoenvironmental reconstruction of the Lower Triassic in the Tanoumri section (B and C, respectively for arid and semi-arid/subhumid climates) and in the Aït Tamlil section (D and E, respectively for arid and semi-arid/subhumid climates). See Figures 6, 9 and 10 for the sedimentary details and stratigraphic position of F3a and F3b subunits. See Table 3 for the facies association codes.

Figure 12: Simplified stratigraphic logs of the Upper Permian - Lower Triassic - Middle Triassic series in Europe (Bourquin et al., 2011), in Argana and MHA basins (This study). Note that dashed zones represent a sedimentary hiatus, and unconformities are shown as sinuous lines. The absolute time scale is taken from the international Commission on Stratigraphy (Gradstein et al., 2008).

Table captions

Table 1: Lithofacies of the Irerhi, Tanoumri and Aït Tamlil sections (modified after Miall, 1977, 2006; Postma 1990; and new codes).

Table 2: Typology, lithology, and interpretation of the various palaeosols. Codes with capital letter "P" which indicates "Palaeosol" and lowercase suffix letter designating the type of paleosol: "c" for calcisol; "v" for vertisol and "g" for gleysol.

Table 3: Facies associations, sedimentary architectures, and depositional environments of the late Permian, Early Triassic, and early Middle Triassic, in the Argana and Marrakech High Atlas basins. See Table 1 for the facies codes and depositional processes.

Declaration of interests

☒The authors declare that they have no known competing financial interests or personal relationships that could have appeared to influence the work reported in this paper.

☐The authors declare the following financial interests/personal relationships which may be considered as potential competing interests:

Table 1: Lithofacies of the Irerhi, Tanoumri and Aït Tamlil sections

Facies Code	Lithofacies	Sedimentary structures	Interpretation
	Conglomerates		
Gm	Dominant quartzite and subordinate quartz fine pebbles to fine cobbles, moderately to poorly sorted, clast- to matrix-supported	Massive, ungraded. Irregular beds with erosive base, up to 80 cm-thick and m-length.	Lag deposits in troughs: gully-fill deposits.
Gmi	Very fine to fine carbonate pebbles (glaebules) to granules, few millimetric bone fragments, moderately sorted, clast- to matrix-supported	Massive monogenic conglomerates. Beds with slightly erosive base, up to 30 cm-thick beds and up to 100 m-length.	Mass flow deposits of reworked calcrete intraclasts, formed during floodplain degradation-aggradation phases, related to fluctuated ground water level.
Gmm	Sub-angular to sub-rounded granules, pebbles, cobbles, poorly sorted, matrix- to clast- supported	Massive to weak grading, chaotic pebbles or imbricated texture with subordinate sandy to silty intercalations (Sm). Beds with flat to irregular base, cm- to 1.5 m-thick.	Debris to mud flow, hyperconcentrated flow, forming levees or lobes, interstratified in proximal alluvial fan.
Gh	Sub-angular gravels to pebbles, moderately to poorly sorted, matrix- to clast-supported	Horizontal bedding to Low angle (< 15°) cross-strata, with, few clast imbrications. Beds up to 50 cm-thick and dam-length.	Stream flow, upper flow regime sheetflooding or decrease of sediment supply, plan-beds.
Gt	Sub-rounded gravels to pebbles, moderately to poorly sorted, matrix-supported	Fining-up sequences with trough cross-bedding. Erosional base.	3D dunes migration.
Gp	Sub-angular gravels, moderately sorted, matrix - supported	Planar cross-bedding.	Migration of 2D dunes Gravel bars.

Ga	Sandy fine to coarse pebbles	Simple planar cross-bedding, individual laminae dip is from 8 to 18°, with some imbrications. Beds with sharp planar base and top, 15 to 50 cm-thick and 1 to 6 m-length.	Antidunes (or backsets) migration under upper-flow-regime sheet flood.
	Sandstones		
Sm	Medium to fine-grained sand, moderately sorted	Massive, dewatering structure or faint lamination. Sharp basal boundary	Deposition from rapid sedimentation, hyperconcentrated flows and/or destruction of primary structures by bioturbations, liquefaction.
	Sl Coarse, medium to fine-grained-sand	Low-angle (< 15°) cross-bedded sandstone.	Humpback or washed-out sand flat of higher stream power.
	Sr Medium, fine to very fine-grained sand	Ripple cross-laminated sandstone.	Current ripples, migrating under lower flow regime.
Sh	Medium to very fine-grained sand, moderately to poorly sorted	Horizontally laminated sandstone, sometimes with parting lineation and flute casts.	Plane-bed from fast, shallow flow in upper flow regime.
Sp	Medium to fine-grained sand	Planar cross-bedded sandstone.	2D dunes migration.
	St Coarse, medium to fine-grained sand	Trough cross-bedded sandstone.	3D dunes migration.
Shg	Medium-grained sandstone and subordinate micro-conglomerate	Mottled horizontally bedded sandstone, massive upper part with infra-millimetric to 2 cm carbonate nodules and topped by mm to cm laminar carbonate. Subordinate cm-thick microconglomeratic beds.	Distal sand flat deposited by sheet flooding with the development of mottling and carbonate nodules attesting the rising of the ground water.

Sg/S	Very coarse-grained sand with dispersed gravels, poorly sorted, matrix –supported, alternate with medium to fine sandstone beds	Alternations between planar-stratified coarser and finer sandstones Beds of 10-25 cm-thick.	Coarse-fine planar-stratified couplets (Planar gravely sandstone/medium to fine sandstone couplet) deposited by upper-flow sheet-flooding.
So	Oolitic medium-grained sandstone	Sandstone with scattered ooliths, wave/current ripples, with sometimes rootlets. Beds with flat base and irregular convex surfaces at the top, of 1 to 3 m-thick and 40 m- length	Oolitic sandstone lobes built under wave effect, foreshore side lobes.
Sq	Medium-grained sand, well sorted, micritic to sparitic cement.	Quartz grains are sub-to rounded shape, polished and gleaming surfaces, with sharp to diffuse contact with interbedded pedogenic and palustrine carbonates.	Reworked and brewed eolian quartz grains by the margin-lake waves.
Sb1	Medium to fine-grained sandstones	Sedimentary structure disturbed by vertical to horizontal burrows characterized by lined and unbranched trace; scratchs are main features as external ornamentation consisting of short longitudinal ridges. Their fills composed of chevron-laminated to meniscate sediment.	Typical of subaqueous environment attributed to Scoyenia characterizing the change in sediment consistency during a hiatus.
Sb2	Fine siltstone to sandstones	Sedimentary structure disturbed by curved cylindrical burrows, unlined and unbranched. The burrow fill is compartmentalized and shows arched menisci.	Taenidium Barretti.
DL	Quartzite or Quartz, coarse pebbles to fine cobbles, moderately to well sorted	Monogenic conglomerates, with mainly quartzite clasts (2 to10 cm) and some quartz clasts (1.5 to 3 cm), horizontally aligned. Clasts are composed of ridges and facets with sometimes smaller-scale pits and grooves. Facet angles from	Deflation lag surface, clasts are shaped by the erosive action of windblown sand forming ventifacts or wind-polished stone. Ventifacts are often reworked by debris flows as levees or lobes.

		the horizontal are 38° – 55°. Beds with sharp basal boundary up to 40 cm-thick.	
Ad	Medium to fine-grained sand, well sorted	Solitary tabular cross-bedded sandstone with foresets dipping 28 – 30° and inverse graded laminae. Beds are 25 to 120 cm-thick and 2.5 to 30 m-length.	Aeolian dunes: grouped tabular cross-bedded sets, mostly similar dip direction of foresets.
Ah	Medium-grained sand, well sorted, well rounded quartz	Horizontally or low angle laminated sandstone with inverse graded laminae.	Dry interdune deposits or aeolian sand sheet deposited under an upper flow blowing wind or characterizing a decrease sand supply.
Ar	Medium-grained sand, well sorted, well rounded quartz	Inversely graded ripples cross-laminated sandstone, that form inclined foresets of 25°. Beds of few cm to 20 cm-thick and 1 to 3 m- length.	Wind ripple, interpreted as aeolian drift deposit in some sections
AM	Sandstones and gravel	Fine wavy laminations, dark in color, forming bands mm to cm and extend over 30 cm, some grains are trapped and upright. Up to three sets of tapered cracks with < 1mm to 6 mm width indicate multiple shrinkage cracks.	Algal mats, stromatolites.
Carbonates			
Cpa	Carbonate beds, micrite to microsparite	Massive to crudely laminated carbonates with often horizontal desiccation cracks or isolating elongated, rounded or angular micritic fragments formed by a network of desiccation cracks (brecciation). Beds of up to 20 cm-thick, frequently interstratified with Cpe.	Carbonate of a lake-margin: the original lacustrine carbonate is modified by desiccation cracks.
C	Carbonate	Massive to crudely	Pedogenic carbonates at

pe		beds, micrite to microsparite	laminated carbonate with alveolar-septal structures, vertical desiccation cracks, sparitic coated grains. Beds of up to 20 cm-thick, frequently interstratified with Cpa.	the top of the nodular horizons, vadose setting.
Ol	**C**	Oolitic limestone, sand-sized, well-rounded and spherical ooids	Horizontally to very low angle laminated or massive with some algal mat structures and glistening/blunted to rounded quartz grains. Beds of 3m-thick and about 100 m-length.	Oolitic shoal.
Or	**C**	Oolitic limestone: oolitic grainstone and oosparite, sand-sized, well-rounded, well-sorted and spherical ooids	Wave, current ripples or laminations with some algal mat structures. Lenticular beds up to 40 cm-thick and tens of meters in length.	Oolitic lobes, shoreface side lobes.
	Heterolithic			
C	**C/**	Interbedded carbonate and clay intraclasts	Laminated carbonate (light brown micrite, microsparite) and dark brown brachiated claystone fabric, sparitic desiccation cracks. Beds of up to 30 cm-thick.	Lacustrine carbonate of lake margin subject to pedogenic processes during aerial exposure phases.
/S	**G**	Interbedded of very fine to medium pebble, angular to sub-angular, poorly sorted, matrix and clast-supported and pebbly medium to coarse sandstone	Alternations of planar-stratified coarser and finer grains with imbricated gravel fabric. Sandstone beds are structureless at the base (Sm) and laminated at the top (Sh). Beds of 3 to 40 cm-thick.	Coarse-fine planar-stratified Couplets (Planar gravel/sand couplet) deposited by upper-flow sheet flooding.
	Mudstones			
m	**F**	Mudstone	Massive.	Deposition from suspension load.

Fsm	Fine silt, silty- or sandy- clay	Pedogenically altered.	Overbank and/or waning flow deposits in standing water-bodies or abandoned watercourses.
Fl	Fine silt, silty- or sandy- clay interbedded with beds of fine to medium sand	Massive or horizontally laminated mudstone interbedded with massive, horizontally or ripple cross-laminated sandstone sometimes bioturbated.	Deposition from suspension alternating with overbank or waning flood.
Flo	Fine silt to silty claystone interbedded with lenses of fine to medium sand and containing scattered oolites	Massive and crudely laminated with scattered ooliths and locally wave ripples, some stromatolithes.	Coastal plain.

Table 2: Typology, lithology, and interpretation of the various palaeosols.

Code	Lithology	Interpretation
Pc	Calcretes developed in mudstone, sandstone or conglomerate host rock, and characterized by upward-increasing carbonate content. In mudstone host rock, three horizons from the base to top are recognized: -wedge-shaped slickensides (Bss) -up to 1 cm carbonate nodules (Bk) -a gradual base and abrupt top of carbonate cemented siltstones associated sometimes to the scattered carbonate nodules (Bkm).	- Calcisol (Tabor et al., 2006) - Aridisol (Soil survey Staff, 2022; Tabor and Montanez, 2004) and as: - Type H of Tabor and Montanez (2004). The progressive transition from nodular to massive and laminar calcretes indicates the decrease of the sedimentation rate (Alonso-Zarza et al., 1999; Wright and Marriot, 1996). These calcretes are typical of semi-arid climate where type I to VI of Machette, 1985 characterized stages of development in increasingly dry seasons.

	In sandstone or conglomerate host rock: only Bk/Bkm horizons are present showing several calcitic shapes which characterize six stages (PC-I to PC-VI): - Stage I: with only micritic filaments (Pc-I), - Stage II: circular to ovoid carbonate nodules shape (Pc-II), - Stage III: coalescing nodules into vertical prism and carbonate matrix (Pc-III), - Stage IV: laminar horizons, sometimes with deformed shape (Pc-IV), - Stage V: laminar carbonates and coated carbonate fragments (Pc-V), - Stage VI: thick hard pan and brecciation (Pc VI).	

P v	Clay soils with carbonate nodules (stages II and III). The lowermost part of the profile displays local laminated mudstones associated sometimes to burrows (tubules: mm to 1 cm long). In clay soils characterised by the non-cumulative (simple) palaeosols: The aggregated mudrock consists from the top to base: - cracking upper horizon (H3), - wedge-shaped peds or aggregates with clay-skin coatings and slickensides horizon (H2), - carbonate in the lowest horizon (H1) (nodules <1cm to 6 cm in diameter).	- Vertisols (e.g., Retallack, 1988; Smith and Kitching, 1997; Tabor and Montanez 2004, Marriott and Wright 2004, Marriott et al., 2005; Marriott and Wright, 2006), - Vertisols type G (Tabor and Montanez, 2004) - Calcic vertisols (Marriott and Wright, 2006; Gastaldo et al. 2020) Geomorphologic setting is mainly flat regions but the gentle slopes are possible (Retallack 1997). The Gmi facies, which covers the profile, records the degradation-aggradation phases in the floodplain. 90% of vertisols form in dry tropical to subtropical environments and 70% in the semi-arid tropics (Caudill et al., 1996). Vertisols occur in subhumid – semi-arid climates with a pronounced dry season according to Geibler and Freiberg (1998), and semi-arid to arid climate according toTabor and Montanez (2004).

	In cumulative palaeosols, the horizons are not separated but cumulated as H2-H1 or H3–H2. In some case the Pv soil is overlain by Gmi facies that can completely remove the horizon H3.	
Pg	Root traces, mottled horizons, Fe-oxide nodules and slickensides, mainly identify in the Fsm facies and subordinately in the Fm, Fl and Sr facies. Gleyed or mottled horizon shows abundant redoximorphic concentrations (grey, yellow and reddish-brown) and reductions with gleyed matrix colours.	Hydromorphic soils-gleying (Retallack, 1988, Tabor and Montanez 2004). Gleyed matrix is induced by gradual depletion of Fe – (Mn) under evidence of periodic water-logging, anoxic conditions and mobilization (Soil Survey Staff, 1975). Episodic water-logging is from flooding events proximal to stream corridors (Tabor et al, 2006). They occur in tropical, humid climate, with high rates of chemical weathering, according to Tabor and Montanez (2004).

Table 3: Facies associations, sedimentary architectures, and depositional environments of the Permian-Early Triassic-early Middle Triassic, in Argana and MHA basins.

Facies Associations	Sedimentary architecture	Depositional environment

FF: Gp, Gh, Sm, Sh, Sp, Sr, Pg, Fl, Fm, Fsm, Pv, Pc, Pg, Sb2	Extensive flat sheet bodies of mainly fine to medium-grained sandstones to siltstones with sharp base and flat to undulatory top (Sm, Sh, Sp, Sr), more rarely conglomerate (Gp, Gh) with erosive base, evolving vertically: - to mudstones (Fl, Fm or Fsm) with paleosol (Pg, Pv, Pc-II and -IV) Isolated or amalgamated beds of 0.1 to dam-thick and of dam to 600 m-length. Sb2 (Taenidium Barretti) is the common bioturbation.	**Distal fluvial fan** distributary system (e.g., Arzani, 2005; Tooth, 2000, 2005; Fisher et al., 2007, 2008; Cain and Mountney, 2009; van Toorenenburg et al., 2016) , commonly named frontal splay characterized by frontal sheetflood events, recording paleocurrent oriented to the main stream flow which grade into floodplain deposits (Fm, Fs, Fsm) which can develop sols and nodules attesting the rising of the ground water, in poorly drained alluvial soils (e.g., Kraus and Aslan, 1993) and under arid to semi-arid climate from paleosol analysis (Table 2).	***Distal fluvial fan (FF)***

FP: Fl, Fm, Fsm, Fv, Gmi, Sr, Pv, Pc, Pg	Interbedded of: - extensive mudstone beds, few cm to 10 m-thick, frequently massive (Fsm) and laminated (Fl) and rarely massive (Fm, Fsm) - very-to fine-grained sandstone and siltstone, sheet-like with a lateral extent of more than 100 m characterized by rippled laminations (Sr) of about 10 to 60 cm-thick. Primary structures can be disturbed by mottled horizons (Pg) or by intense pedogenic features (Pv or Pc-II, -IV and -V). The Pv soil is sometimes covered by intraformational conglomerates (Gmi) with carbonate nodules clasts.	**Floodplain** deposits with extensive unconfined sheetflood typical of overbank deposits (e.g., Nanson and Croke, 1992; Smith, 1993; Jorgensen and Fielding, 1996; Bridge, 2003; Tooth, 2005) and mainly carbonate soils that attest the seasonal dry climate with contrasting seasons wet/dry (Pv) to the immature or strongly developed aridisols (Pc-II to -V, Machette, 1985). Pg hydromorphic soils-gleying (e.g., Kraus, 1999) is subordinate. The Pv soil associated with Gmi facies formed during floodplain degradation-aggradation phases (e.g., Smith and Kitching, 1997; Marriott and Wright 2006). The FP characterized distal zone within either arid or semi-arid climate.	***Floodplain (FP)***

AFp: Gmm, Sm	Matrix- to clast-supported conglomerates (Gmm) with flat to irregular base grading vertically to sandstones (Sm). Sometimes, the basal part can contain locally ventifacts. Isolated or stacked beds of 40 cm to 1.5m-thick.	**Proximal alluvial fan** with hyperconcentrated flow and debris flow lobes (e.g., Blair & McPherson 1994; Blair and McPherson 1998; Muravchik et al., 2014; Ezquerro et al., 2019).	***Proximal Alluvial Fan (AFp)***

AFm1: G/S, Ga, Gm, Gmm, Sm, Ar, Ah, Pc-II, Pc-IV Pc-V	Planar-interstratified beds of sandy and very fine to medium pebble (G/S), 3 to40 cm-thick associated to backsets or antidunes (Ga), 15 to 50 cm-thick and 1 to 6 m-length, with sharp and planar contacts with: - local gully-fill deposits (Gm) up to 40 cm thick with low-relief scours (up to 10 cm) - occasionally Sm and subordinate debris flow deposits (Gmm). - Pc soils (stage II, mainly IV, rarely V)and sometimes interbedded and aeolian deposits: - planar-cross bedded medium-grained sandstone (Ar); 25° dip foresets, few cm- to 30 cm-thick and 1 to 3 m-length, - horizontally or low angle laminated sandstone (Ah), 10 to 50	**Med-alluvial fan** characterizes by mainly sheetflood gravelly-sandy couplets of ephemeral streams (e.g., Muravchik et al. 2014; Blair, 1987; Chamyal et al., 1997; Sohn et al., 1999; Mather and Hartley 2005; Ezquerro et al., 2010). The Pc soils indicating either semi-arid or more arid climate. The association with Pc-II soil (Table 2) and aeolian deposits attest arid climate condition.	***Medial Alluvial Fan (AFm)***

AFm2: Gt, Gp, Gh, St, Sp, Sh, Sr, Sm, Ar, Ad, Ah, Pc-II	Simple to composite gravely-pebbly to sandy bedload bodies with flat to slightly irregular base (Gp-Gh, Gh low angle-Sh, Gp-Sh, Gp-Sp-Sh, Gp-St, Gp-Sm, Gh-Sp-Sh-Sr, Gt-Sm, Gt-Sm-Sh-Sr, Gp-Sp-Sh, Sm-Sh, Sh-Sr or stacked Sp associations) up to 2 m-thick, associated sometimes with: - planar-cross bedded medium-grained sandstone (Ar); 25° dip foresets, few cm- to 30 cm-thick and 1 to 3 m-length (Ar) and - Pc soil of stage II. AFm2 can be associated with Ad and/or Ah facies (ER facies association)	**Med-alluvial fan** dominated by stream flow with 2D/3D type bedforms as gravely or sandy bars interstratified or isolated (e.g., Makhlouf et al. 2010; Blair 1987) with Pc soils indicating either semi-arid or more arid climate. The aeolian wind sandstone or aeolian drift with opposite wind flow direction and arid soil attest arid-alluvial plain	
AFm3: Sg/S, Sm,	Stacked of planar-stratified sandy couplets	**Med-alluvial fan deposits** characterize mainly by the	

Pc-IV	(Sg/S), 20 to 80 cm-thick sometimes, with occasionally massive sandstones (Sm) associated with–mature soil Pc-stage IV.	sheetflood sandy couplets–with mature soil that attest semi-arid-alluvial plain (e.g., Chamyal et al., 1997; Sohn et al., 1999).	
AFd: Sm, Sp, Sh, Sl, Shg, Sr, Fl, Fm, Fsm, Pc, Pg	Interbedded of: - mainly superposition of medium to fine sandy sheet (Sm, Sp, Sh, Sl, Shg, Sr) with flat base and generally undulating to rippled top, up to 1.30 m-thick, 10 m to 100s m-length - mudstones (Fl, Fm, Fsm) with Pc and Pg soils.	**Distal alluvial fan deposits**, the sandy sheet floods are locally interstratified within alluvial plain facies (e.g., Miall 1996; Blair, 2000; Mather & Hartley, 2005; Ezquerro et al., 2019) composed of unmodified to modified soils Pc or hydromorphic soil (Pg, Table 2) which attest either arid or subhumid climate.	***distal Alluvial Fan (AFd)***

RE: DL	Quartzite or quartz pebbles to cobbles aligned on more or less continuous surface clasts, sharp base and extended to 100 m.	**Reg deposit** or desert pavement, the wind-blow abrasion winnowed the fine fraction and shape ventifacts or wind-polished stone (e.g., Durand and Bourquin, 2013).	***Aeolian deposits***

ER: Ad, Ah	Either: - solitary tabular cross-bedding sandstone (Ad), sets are 25 to 120 cm thick and cosets are 0.50 to 3 m thick and 30 m to 2 km extent. - horizontally or low angle laminated sandstone (Ah), 60 cm -3m thick and more than 200 m of extent, Or interstratified Ad and Ah facies, up to 6 m-thick and 2 km-length. The base is frequently lined by less than 3 cm rich quartz ventifacts	**Erg deposits**: the dune deposits (Ad) can alternate with aeolian sand sheet deposits (Ah) representing the dry interdune and attest of a high regime wind blowing or a decrease of sand supply (e.g., Clemmensen and Abrahamsen, 1983; Spalletti et al, 2010; Brookfield and Silvestro, 2010).	
PA: Cpa, Sq, Cpe, C/C, Pg	Three facies associations can be observed: - undulatory massive or laminated carbonates with horizontal desiccation cracks and micritic intraclasts (Cpa) interbedded, with diffuse contact, with sub- to rounded polished and gleaming quartz	**Palustrine** depositional environment (e.g., Méndez-Bedia et al., 2020; Alonso-Zarza and Wright 2010a; Alonso-Zarza 2003), i.e., margin lake deposits, composed by either: - interbedded palustrine carbonate and sandstone beds characterizing reworked and brewed aeolian quartz grains by the margin-lake waves. This lake-margin	***Palustrine (PA)***

	(Sq), with Pg soil, - interbedded of carbonate with horizontal desiccation, rounded or angular micritic fragments cracks formed by network of desiccation cracks (Cpa) and pedogenic carbonate (Cpe), with Pg soil and composed from the base to top: - isolated nodular calcretes (3 cm in diameter) are formed in red mudstones, 30 to 50 cm-thick, - vertically elongated carbonate nodules (3 to 20 cm in length, 2 to 6 cm in diameter), 15 to 40 cm-thick, - hard and massive limestone bed intensely brecciated, up to 20 cm thick. - locally (in Tanoumri F2	deposits records expansion-contraction of the lake. - or the water table favored the development of palustrine carbonates between maximum and minimum lake level in a phreatic setting (Alonso-Zarza and Calvo, 2000), i.e. from maximum lake level to landward the pedogenic development are active forming pedogenic calcretes (Cpe) (e.g., Alonso-Zarza 2003; Alonso-Zarza and Wright 2010) at the top of the nodular horizons. The setting is vadose (e.g., Wright and Tucker 1991). Locally, the distal fluvial fan evolves to an alluvial plain with pond or shallow lake deposits of slightly saline mudflats. During aerial exposure phases, palustrine deposits develop in distal zone of fluvial distributary system.	

	Unit) stack of interstratified laminated carbonate and brecciated claystone, with epigenesis of gypsum crystals by calcite (C/C), up to 30 cm-thick.		

L 1: C Or, COl, AM	Planar-laminated and rarely massive structure overlain by undulating cross ripple lamination (COl, COr), few glistening and blunted to rounded quartz grains are dispersed, and Algal mats (AM).	**Oolitic shoal or shoreface lobes** (e.g., Milroy and Wright 2000; 2002; Palermo et al. 2008; Voigt et al. 2011).	***Oolitic shoreline lake (L)***
L 2: S o, Sh, Sr	Up to 5 m thick olitic sandstone (So) interstratified with sandstones (Sh, Sr).	**Foreshore lobes** formed under wave effect (e.g., Milroy and Wright 2000; 2002; Palermo et al. 2008 ; Voigt et al. 2011)	
L 3:	Mainly mudstones (Flo) and subordinate sandstones (Sh, Sr) with scattered ooliths,	**Coastal plain or strand plain** (e.g.,	

Fl o, Sh, Sr, Fm	wave ripples and stromatolithes in mudstones (Fm).	Milroy and Wright 2000; 2002; Palermo et al. 2008 ; Voigt et al. 2011)	
B m: G p, Gh, Sl, AM, Pc-III	Interfingering wedge-planar foresets of sandy and pebbly beds, mainly composed of polygenic to monogenic, intra- and extra-clasts conglomerates (Gp, Gh low angle) with sub-angular to rounded and well- to moderately sorted material, imbrications and sandstones (Sl). Calcite cement, local occurrence of algal mats structures (AM) and of Pc- III soils. Beds with flat and sharp base and convex top bedform, up to 4 m-thick and hundred meters to 1 km of extension.	**Gravel lake shoreline or berm** (shoreline butte), deposited along distal fan and emerged by the lake in humid conditions (e.g., Blair 1999a, 1999b, 2000).	***Gravel lake shoreline***

RB: Gt, Gp	Conglomerate beds are mainly monogenic conglomerate, with few imbricated pebbles with low-relief erosive base and more or less irregular top The common facies associations are: stacked Gt, Gt, Gp, and stacked Gp. Beds up to 4.2 m-thick and hundred meters of extension.	**Braided rivers**: channel and bar bedforms (e.g., Miall, 1977, 1978, 1996; Medici et al., 2015; Mukhopadhyay et al., 2016).	***Braided river (RB)***

RM -Gm, Gt, Sp, Sr, Sb1	Sandstone sheets are 1 to 2 m-thick and more than 40 m-wide, Composed of coarse to medium-grained sandstone, moderately sorted (Gm, Gt, Sp and Sr), Epsilon cross bedded. Scoyenia (Sb1) represents the common associated bioturbation.	**Meandering river:** point bar deposits in the meandering system (e.g., Gugliotta et al 2018; Ghazi and Mountney, 2009; Viseras et al., 2006).	***Meandering river (RM)***

Graphical abstract

Highlights

- The late Permian, Lower to early Middle Triassic sedimentation through the Argana and Marrakech High Atlas basins.
- Evolution from aeolian, alluvial fan, lacustrine to meandering rivers deposits under change climate conditions.
- P-T and Lower-early Middle Triassic angular unconformities associated to direction drainage change.
- Comparison with European basins reveals similar unconformities and a similar climate evolution.

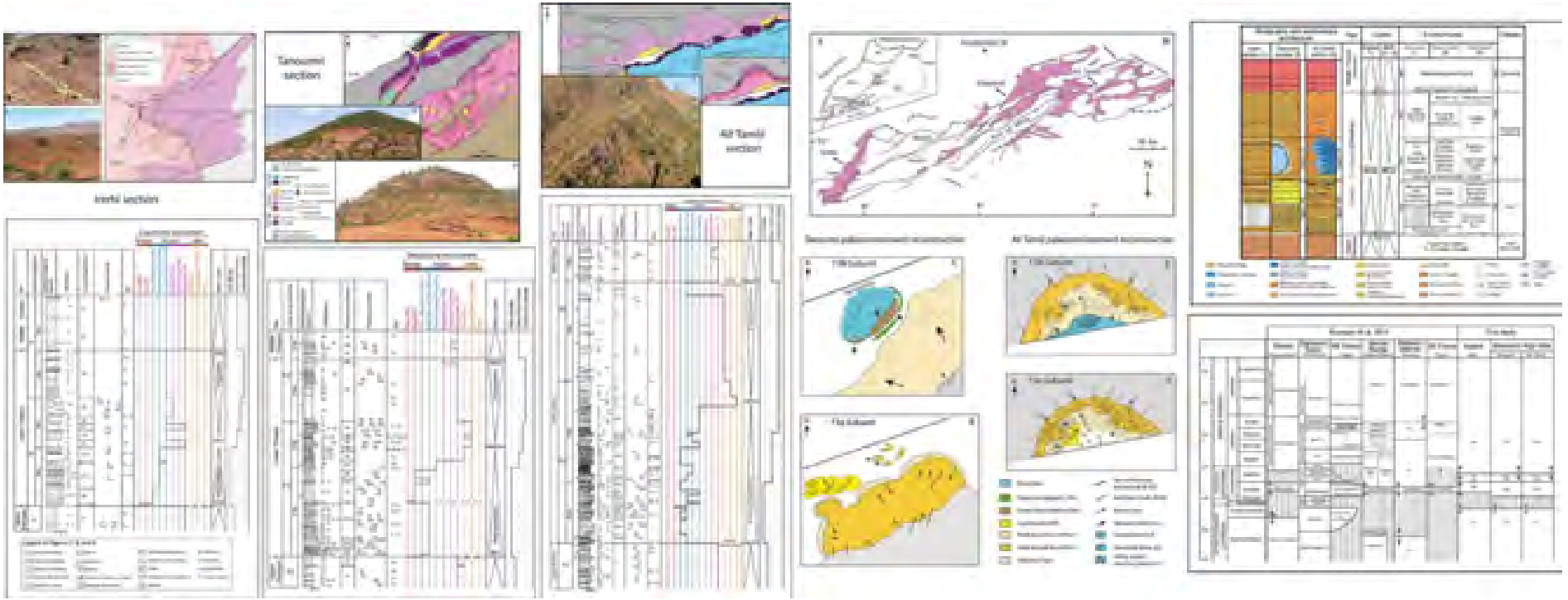

Graphics Abstract

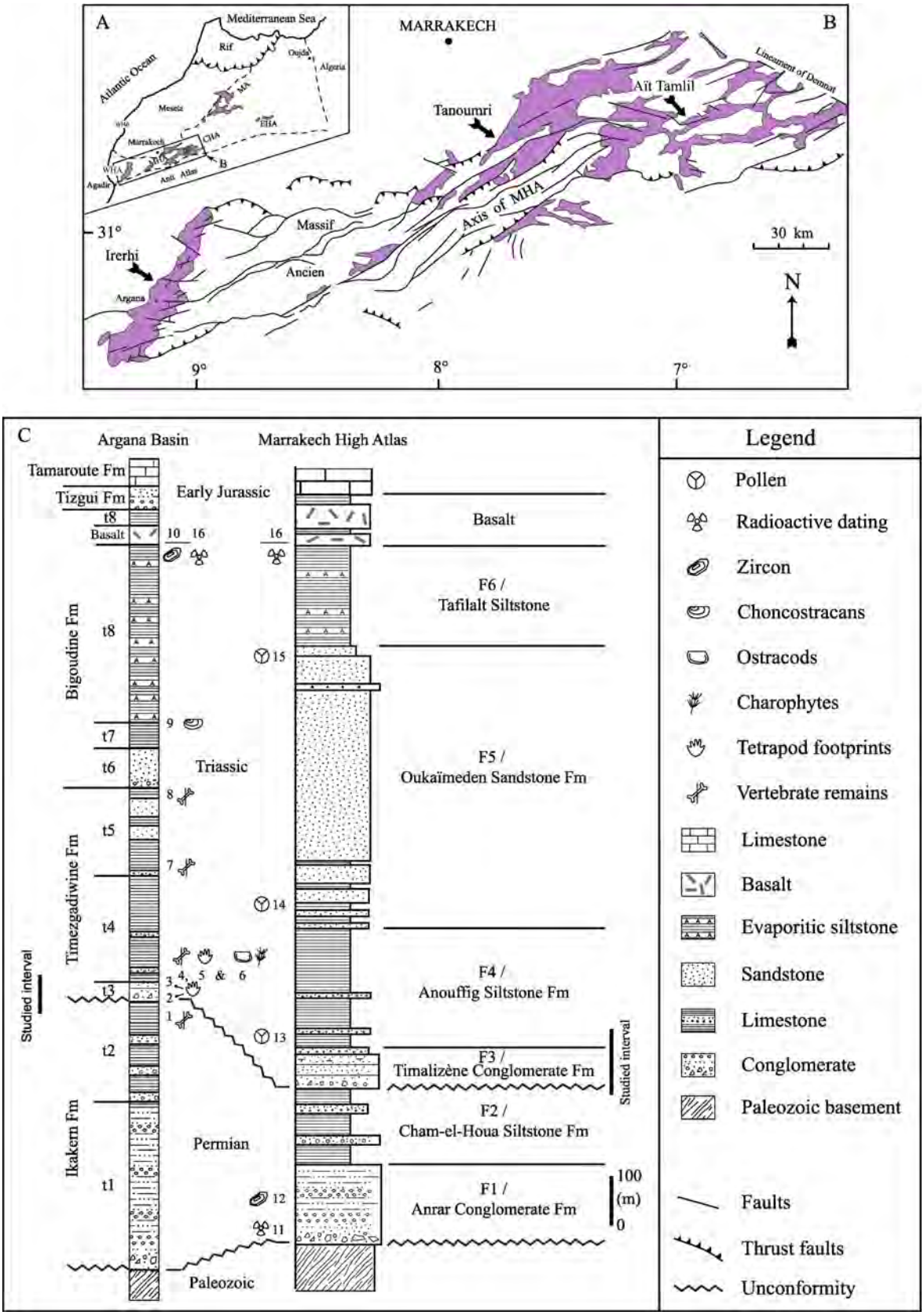
A
Mediterranean Sea
Rif
Oujda
Algeria
Atlantic Ocean
MA
Meseta
EHA
WHA
CHA
Marrakech
Agadir
Anti Atlas
B
MARRAKECH
B
Lineament of Demnat
Aït Tamlil
Tanoumri
Axis of MHA
Massif
Ancien
Irerhi
Argana
31°
30 km
N
9°
8°
7°
C
Argana Basin
Marrakech High Atlas
Legend
Tamaroute Fm
Tizgui Fm
t8
Basalt
Early Jurassic
Bigoudine Fm
t7
t6
Triassic
Timezgadiwine Fm
t5
t4
t3
t2
Ikakern Fm
t1
Permian
Paleozoic
Studied interval
F6 / Tafilalt Siltstone
F5 / Oukaïmeden Sandstone Fm
F4 / Anouffig Siltstone Fm
F3 / Timalizène Conglomerate Fm
F2 / Cham-el-Houa Siltstone Fm
F1 / Anrar Conglomerate Fm
100
(m)
0
Pollen
Radioactive dating
Zircon
Choncostracans
Ostracods
Charophytes
Tetrapod footprints
Vertebrate remains
Limestone
Basalt
Evaporitic siltstone
Sandstone
Limestone
Conglomerate
Paleozoic basement
Faults
Thrust faults
Unconformity

Figure 1

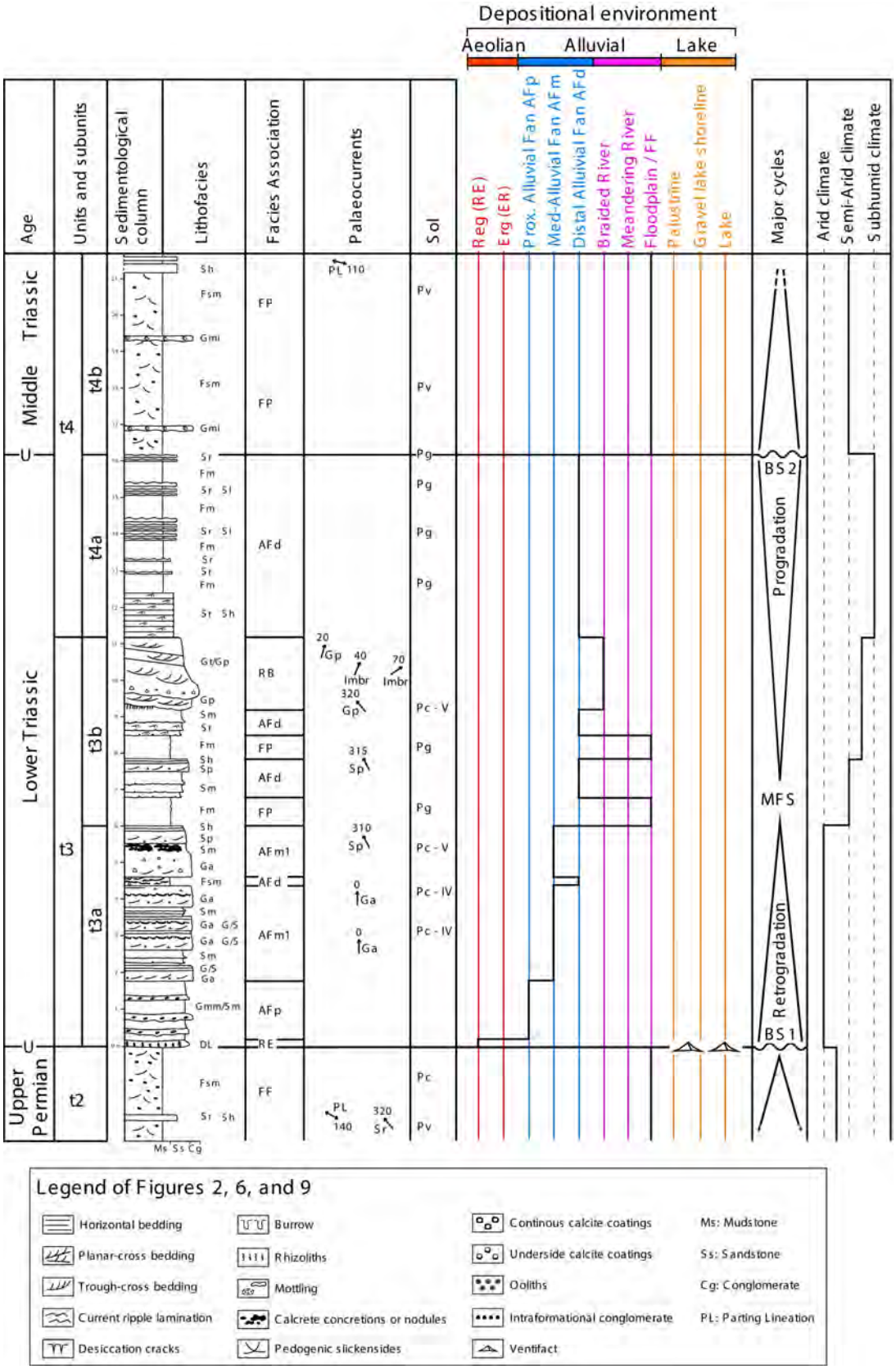
Depositional environment
Aeolian
Alluvial
Lake
Age
Units and subunits
Sedimentological column
Lithofacies
Facies Association
Palaeocurrents
Sol
Reg (RE)
Erg (ER)
Prox. Alluvial Fan AFp
Med-Alluvial Fan AFm
Distal Alluvial Fan AFd
Braided River
Meandering River
Floodplain / FF
Palustrine
Gravel lake shoreline
Lake
Major cycles
Arid climate
Semi-Arid climate
Subhumid climate
Upper Permian
Lower Triassic
Middle Triassic
t2
t3
t3a
t3b
t4
t4a
t4b
BS 2
Progradation
MFS
Retrogradation
BS 1
Ms Ss Cg
Legend of Figures 2, 6, and 9
Horizontal bedding
Planar-cross bedding
Trough-cross bedding
Current ripple lamination
Desiccation cracks
Burrow
Rhizoliths
Mottling
Calcrete concretions or nodules
Pedogenic slickensides
Continous calcite coatings
Underside calcite coatings
Ooliths
Intraformational conglomerate
Ventifact
Ms: Mudstone
Ss: Sandstone
Cg: Conglomerate
PL: Parting Lineation

Figure 2

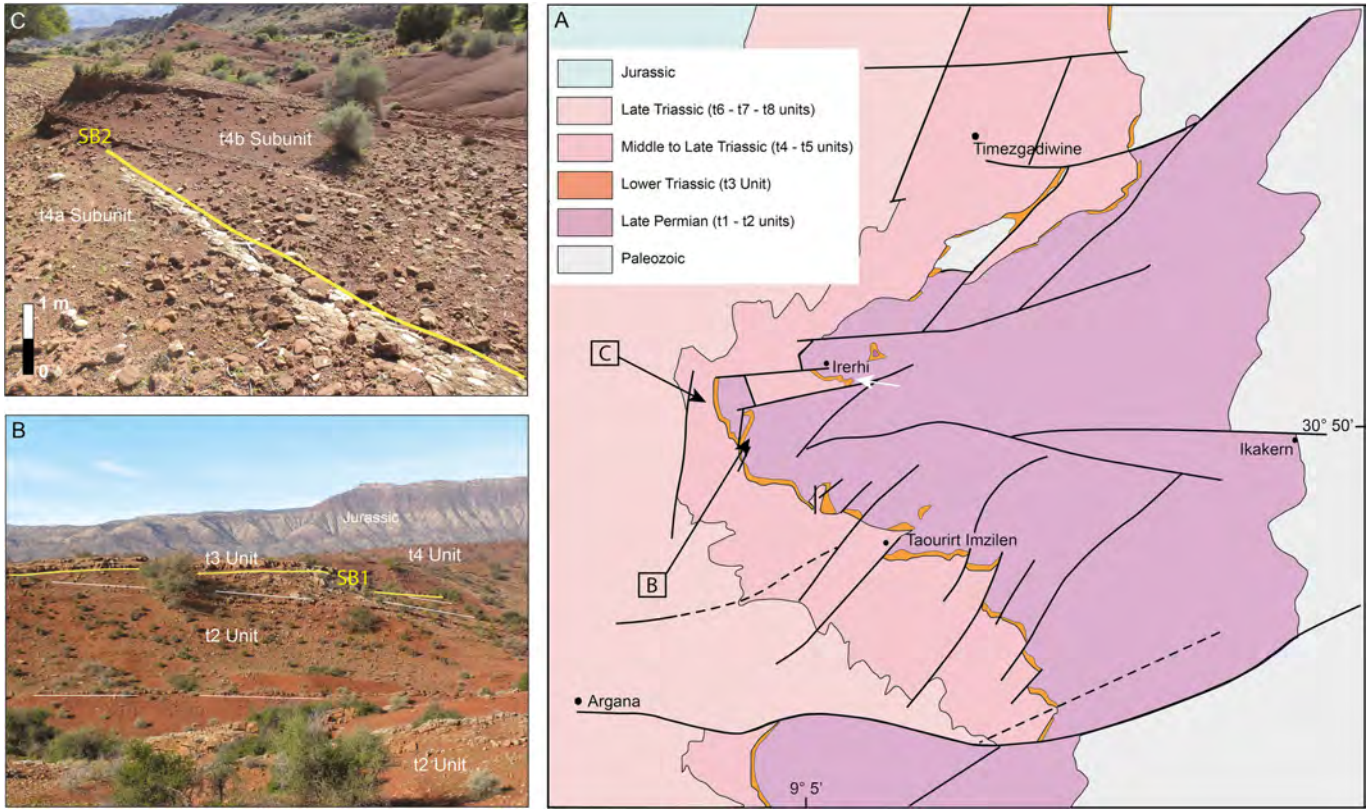
C
SB2
t4b Subunit
t4a Subunit
1 m
0
B
Jurassic
t3 Unit
t4 Unit
SB1
t2 Unit
t2 Unit
A
Jurassic
Late Triassic (t6 - t7 - t8 units)
Middle to Late Triassic (t4 - t5 units)
Lower Triassic (t3 Unit)
Late Permian (t1 - t2 units)
Paleozoic
Timezgadiwine
C
Irerhi
30° 50'
Ikakern
Taourirt Imzilen
B
Argana
9° 5'

Figure 3


A
t4b Subunit
SB2
t4a Subunit
RB
t3b Subunit
t3a Subunit
2 m
0
C
Ga
Sm
G/S
AFm1
B
Sm
Gmm
AFp
D
t4b
t4a
1 m
Pg soil
SB2
0
E
Sl
Sr
AFd
Sr/Fm
t4a Subunit
F
SB1
F3 Unit
F2 Unit
Sm
Fm
Sp
FF
Sh
G
H
C/C
F2 Unit-PA
H
2
1
F2 Unit
J
F3a Subunit
Sm
Gmm
F2 Unit
AFp
RE
SB1
K
Ventifacts
I
Gypsum
F2 Unit
L
Gm
G/S
Ar
F3a Subunit
AFm1
M
Gmm
Ga
Ar
AFm1
F3a Subunit
N
Sm
Shg
Sl
Fsm
AFd
F3b Subunit
P
Pg soil
Gleyed matrix colours
O
Sp
AFd
Fsm
P
PA
Q
F3b Subunit
Q
Cpa
R
Deformed carbonate
Hard carbonate
P
P
Pc-IV/Pc-VI soils
Cpe

Figure 4

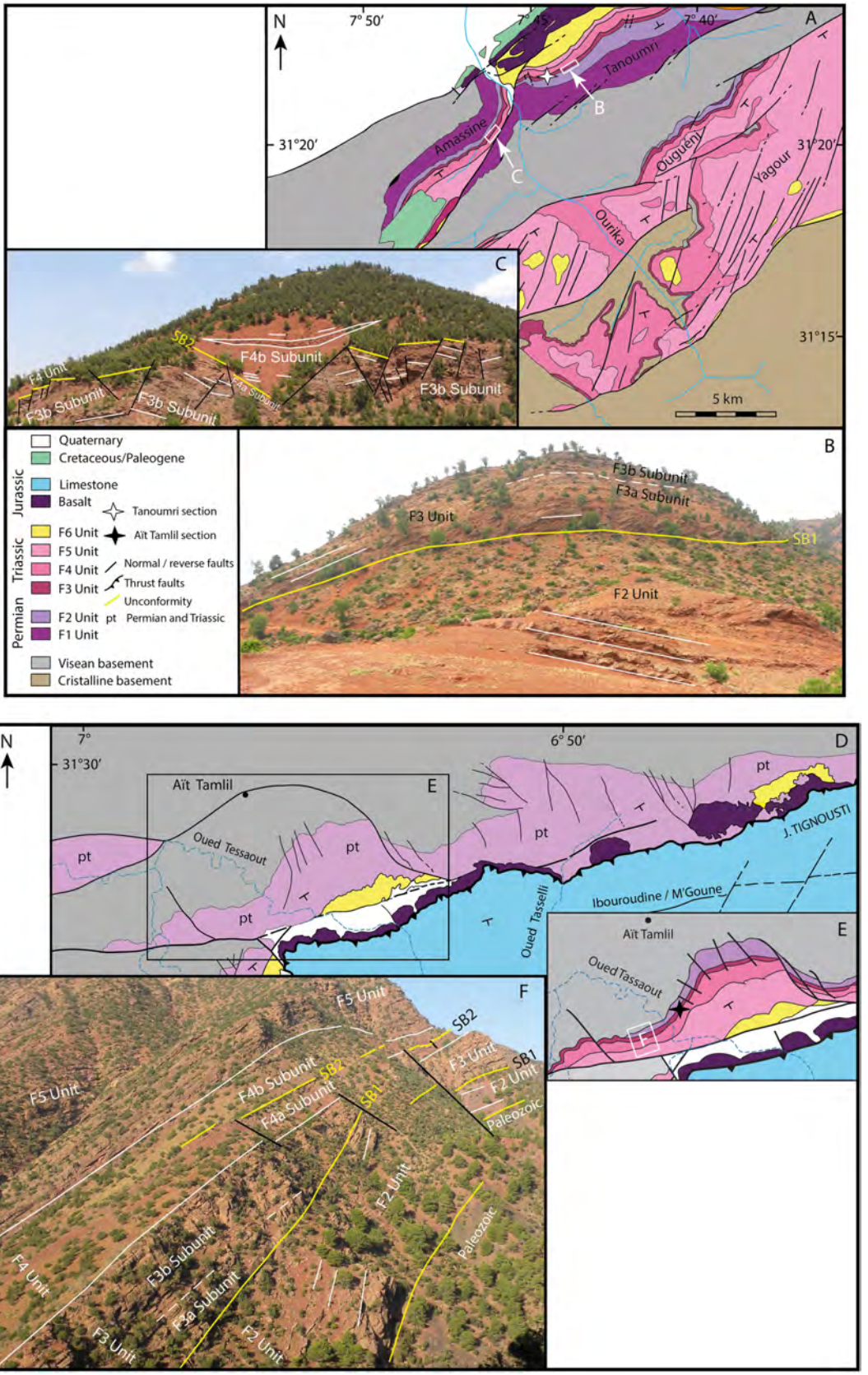
N
7° 50′
7° 40′
A
Tanoumri
B
Amassine
C
31°20′
Ouguenj
Vagour
Ourika
31°15′
5 km
C
SB2
F4b Subunit
F4 Unit
F3b Subunit
F3a Subunit
F3b Subunit
F3b Subunit
B
F3b Subunit
F3a Subunit
F3 Unit
SB1
F2 Unit
Quaternary
Cretaceous/Paleogene
Jurassic
Limestone
Basalt
Tanoumri section
Triassic
F6 Unit
F5 Unit
F4 Unit
F3 Unit
Aït Tamlil section
Normal / reverse faults
Thrust faults
Unconformity
Permian
F2 Unit
F1 Unit
pt Permian and Triassic
Visean basement
Cristalline basement
N
7°
6° 50′
D
31°30′
Aït Tamlil
E
Oued Tessaout
pt
J. TIGNOUSTI
Ibouroudine / M'Goune
Oued Tasselli
Aït Tamlil
E
Oued Tassaout
F
F5 Unit
SB2
F4b Subunit
F4a Subunit
SB1
F3 Unit
F2 Unit
Paleozoic
F5 Unit
F2 Unit
Paleozoic
F4 Unit
F3b Subunit
F3a Subunit
F3 Unit
F2 Unit

Figure 5

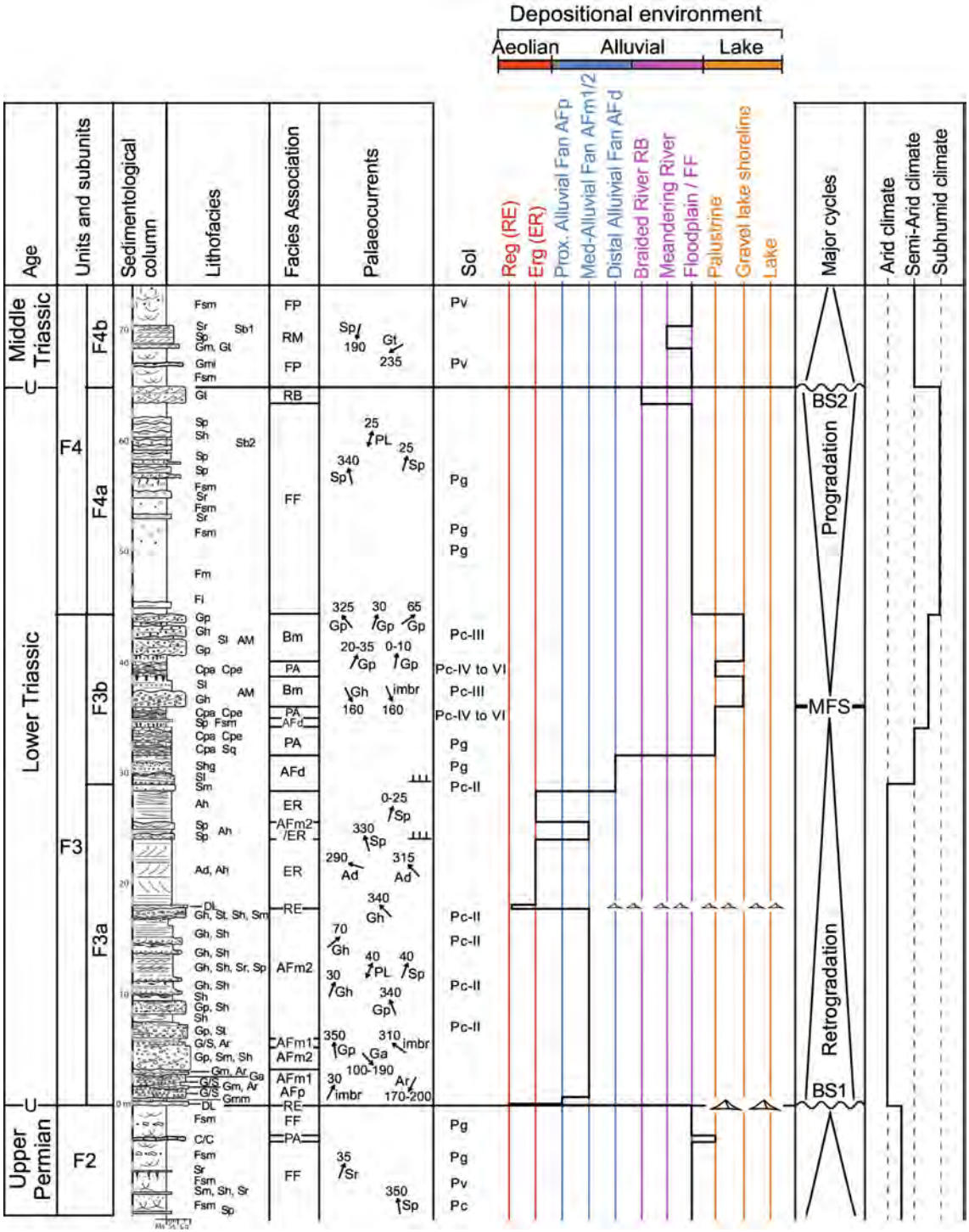
Depositional environment
Aeolian
Alluvial
Lake
Age
Units and subunits
Sedimentological column
Lithofacies
Facies Association
Palaeocurrents
Sol
Reg (RE)
Erg (ER)
Prox. Alluvial Fan AFp
Med-Alluvial Fan AFm1/2
Distal Alluvial Fan AFd
Braided River RB
Meandering River
Floodplain / FF
Palustrine
Gravel lake shoreline
Lake
Major cycles
Arid climate
Semi-Arid climate
Subhumid climate
Middle Triassic
Lower Triassic
Upper Permian
F4
F4b
F4a
F3
F3b
F3a
F2
BS2
Progradation
MFS
Retrogradation
BS1

Figure 6

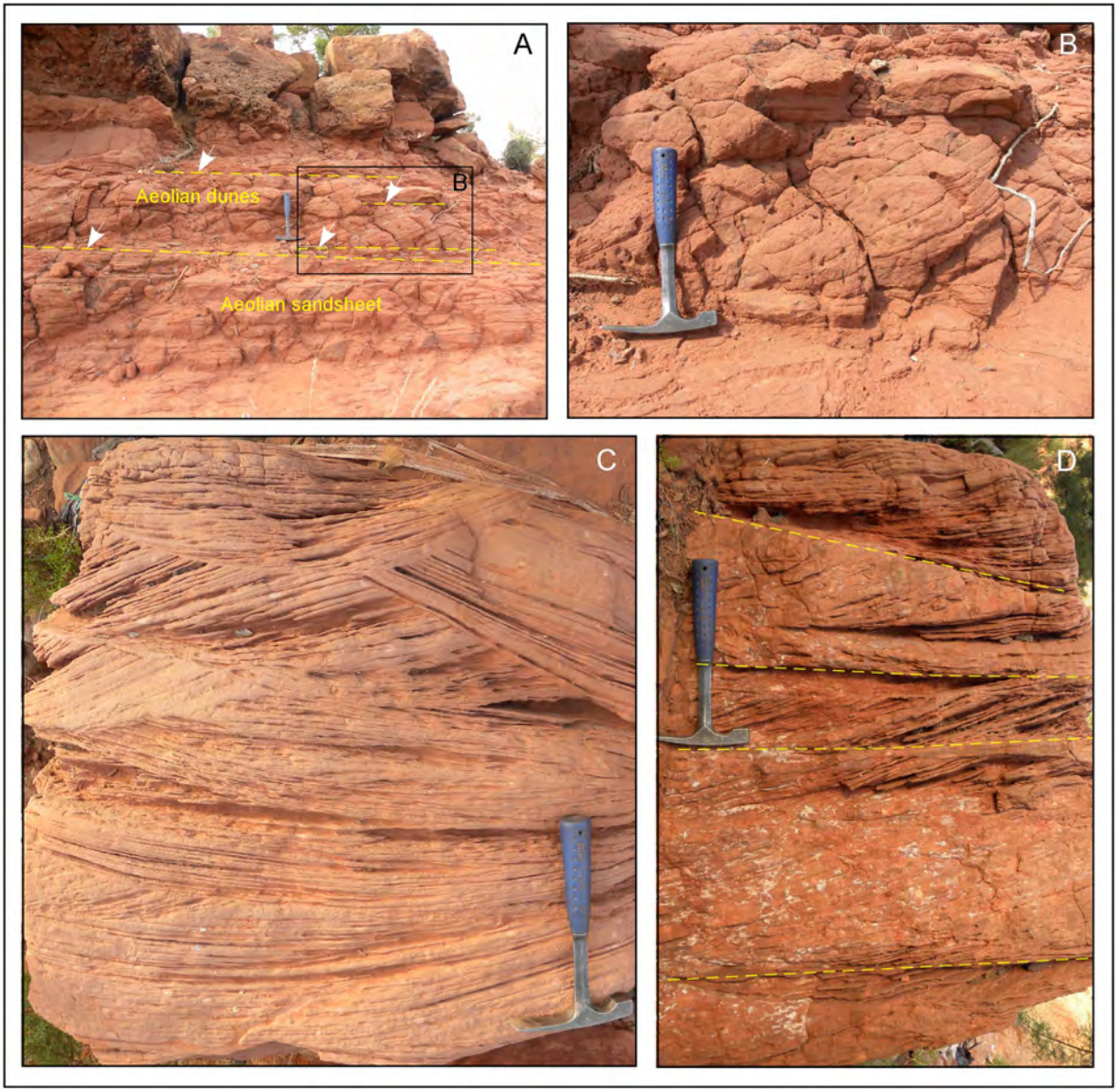

Figure 7


A
Clastic deposit
F3b Subunit
Cpe
B
Sq
shiny-blunt shaped quartz
E
0 mm 12
C
Convex top
Bm
Flat base
Gp
Sl / Gh
PA
1 m
0
F3b Subunit
F
AM
D
0 10 20
mm
G
H
Sb2
4.5 mm
Sh
Sp
Fsm
H
F4a Subunit / FF
I
F5 Unit
F4 Unit
F3b Subunit
F3a Subunit
F2 unit
J
Gp
Gh
Stacked Pc-IV
AFm1/AFm2
K
O
M
L
L1/L2
Sh
Sr
El
Sp
AFd
F3b Subunit
L
COl
L1
5 mm
M
COr
E1
N
AM
O
0 mm 10
P
F5 Unit
Fm
F4b Subunit
F4a Subunit
SB2
Flo
Flo
L3
Q
Fsm
FP
Sr
Fsm
Sp
RM
F4b Subunit

Figure 8

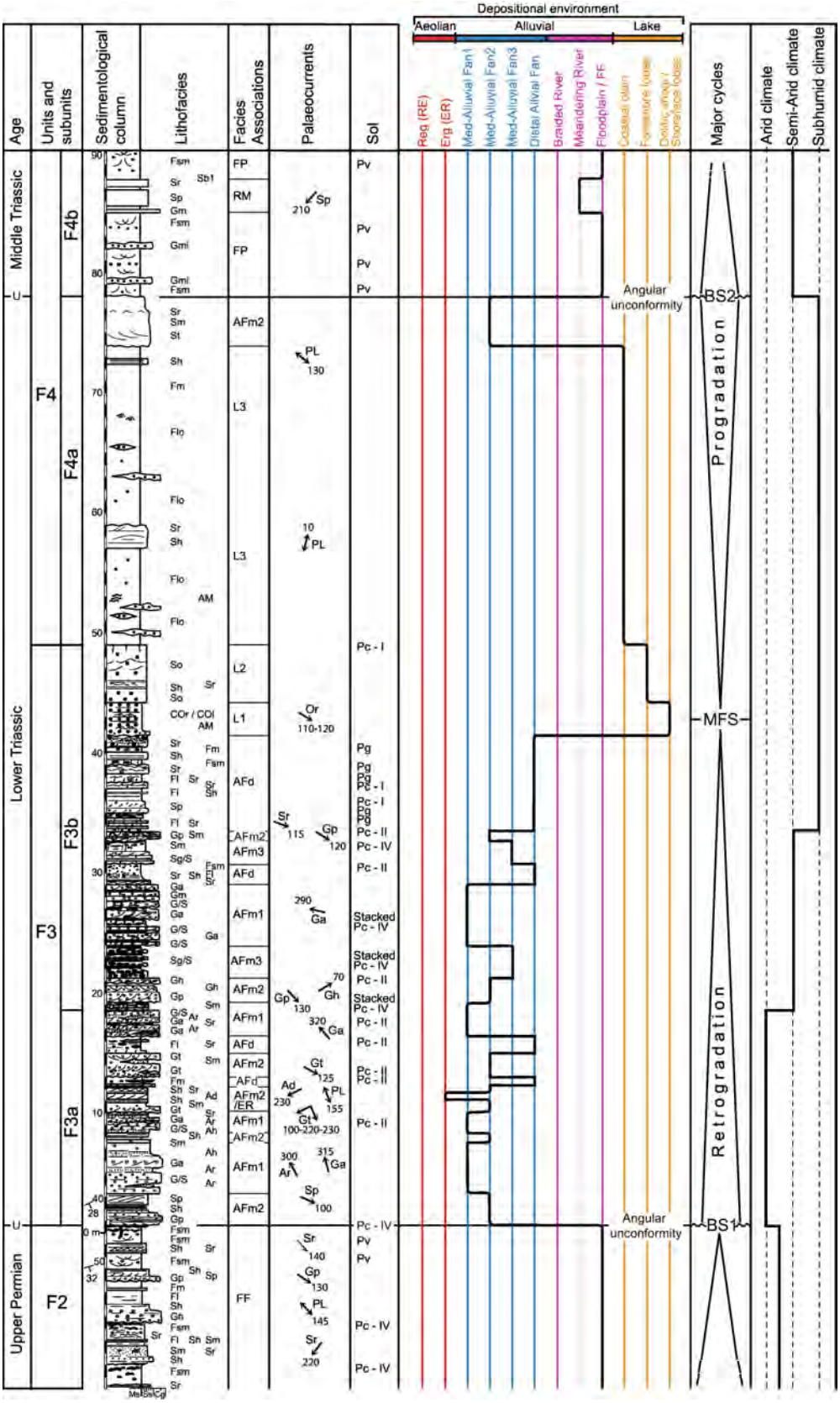
Depositional environment
Aeolian
Alluvial
Lake
Age
Units and subunits
Sedimentological column
Lithofacies
Facies Associations
Palaeocurrents
Sol
Req (RE)
Erg (ER)
Med-Alluvial Fan1
Med-Alluvial Fan2
Med-Alluvial Fan3
Distal Alluvial Fan
Braided River
Meandering River
Floodplain / FF
Coastal plain
Major cycles
Arid climate
Semi-Arid climate
Subhumid climate
Upper Permian
Lower Triassic
Middle Triassic
F2
F3
F3a
F3b
F4
F4a
F4b
Angular unconformity
BS2
MFS
BS1
Progradation
Retrogradation

Figure 9

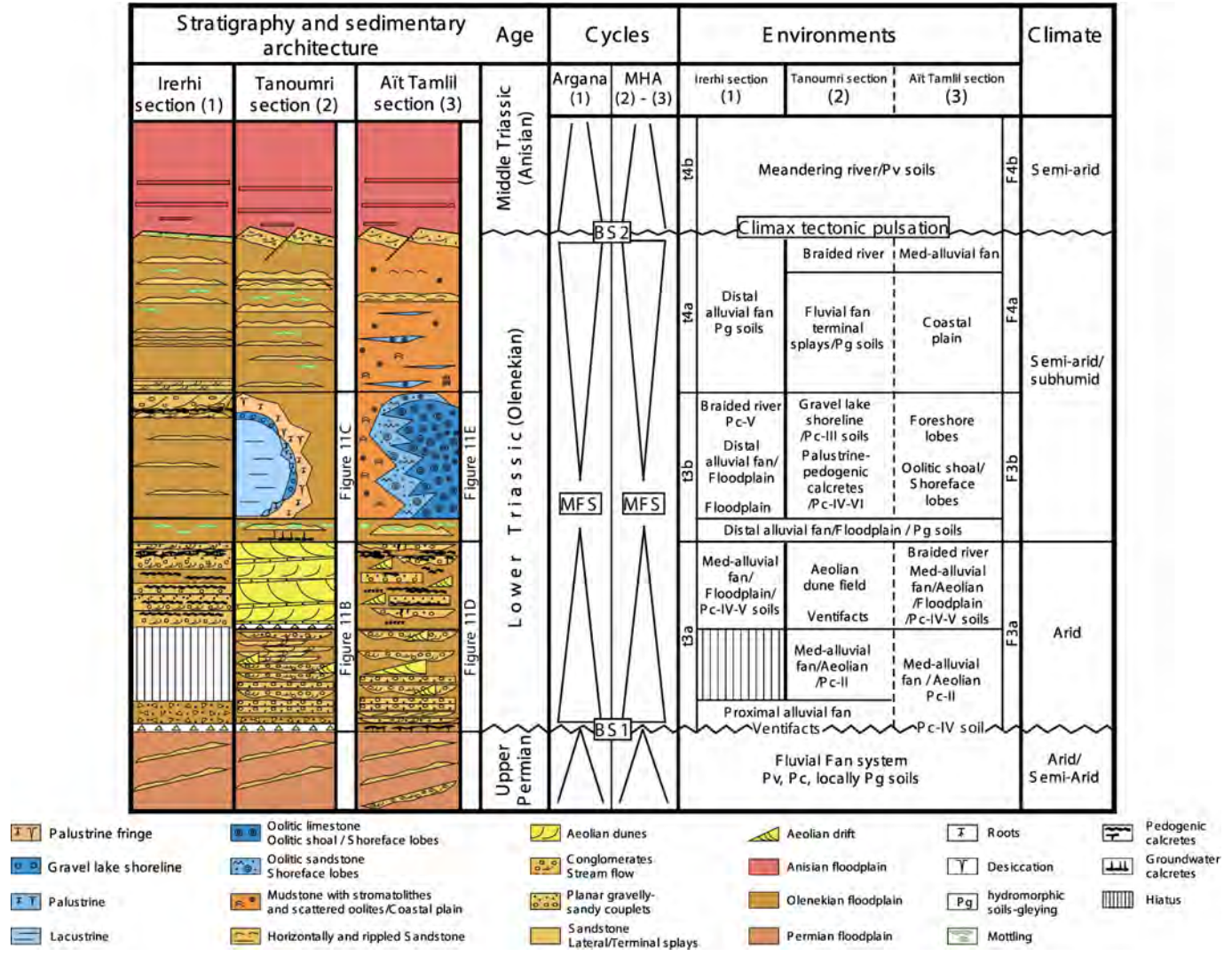
Stratigraphy and sedimentary architecture
Age
Cycles
Environments
Climate
Irerhi section (1)
Tanoumri section (2)
Aït Tamlil section (3)
Argana (1)
MHA (2) - (3)
Irerhi section (1)
Tanoumri section (2)
Aït Tamlil section (3)
Middle Triassic (Anisian)
Lower Triassic (Olenekian)
Upper Permian
BS2
BS1
MFS
MFS
Figure 11C
Figure 11E
Figure 11B
Figure 11D
t4b
t4a
t3b
t3a
F4b
F4a
F3b
F3a
Meandering river/Pv soils
Climax tectonic pulsation
Braided river
Med-alluvial fan
Distal alluvial fan Pg soils
Fluvial fan terminal splays/Pg soils
Coastal plain
Braided river Pc-V
Distal alluvial fan/ Floodplain
Floodplain
Gravel lake shoreline /Pc-III soils
Palustrine-pedogenic calcretes /Pc-IV-VI
Foreshore lobes
Oolitic shoal/ Shoreface lobes
Distal alluvial fan/Floodplain / Pg soils
Med-alluvial fan/ Floodplain/ Pc-IV-V soils
Aeolian dune field
Ventifacts
Braided river
Med-alluvial fan/Aeolian /Floodplain /Pc-IV-V soils
Med-alluvial fan/Aeolian /Pc-II
Med-alluvial fan /Aeolian Pc-II
Proximal alluvial fan
Ventifacts
Pc-IV soil
Fluvial Fan system
Pv, Pc, locally Pg soils
Semi-arid
Semi-arid/ subhumid
Arid
Arid/ Semi-Arid
Palustrine fringe
Gravel lake shoreline
Palustrine
Lacustrine
Oolitic limestone
Oolitic shoal / Shoreface lobes
Oolitic sandstone
Shoreface lobes
Mudstone with stromatolithes and scattered oolites/Coastal plain
Horizontally and rippled Sandstone
Aeolian dunes
Conglomerates
Stream flow
Planar gravelly-sandy couplets
Sandstone
Lateral/Terminal splays
Aeolian drift
Anisian floodplain
Olenekian floodplain
Permian floodplain
Roots
Desiccation
Pg
hydromorphic soils-gleying
Mottling
Pedogenic calcretes
Groundwater calcretes
Hiatus

Figure 10

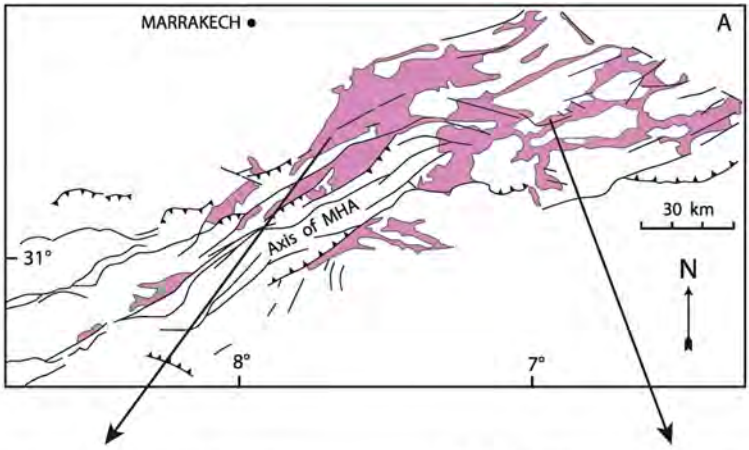

Tanoumri palaeoevironment reconstruction

Aït Tamlil palaeoenvironment reconstruction

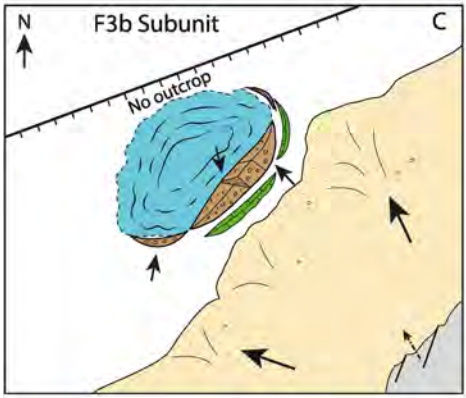

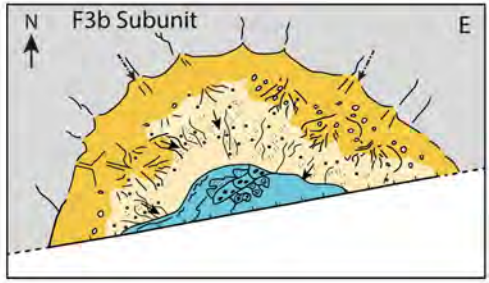

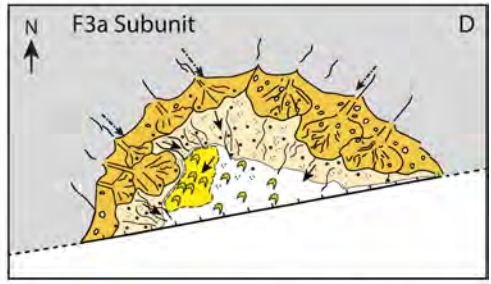

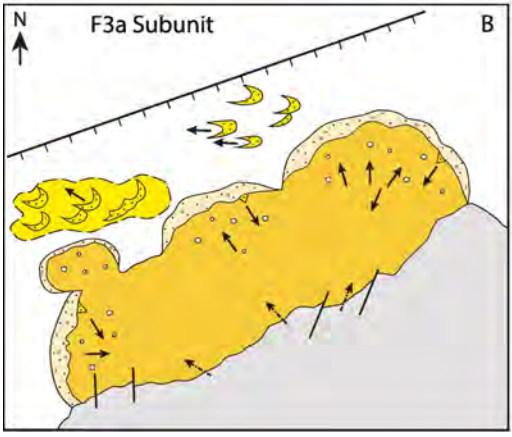

Figure 11

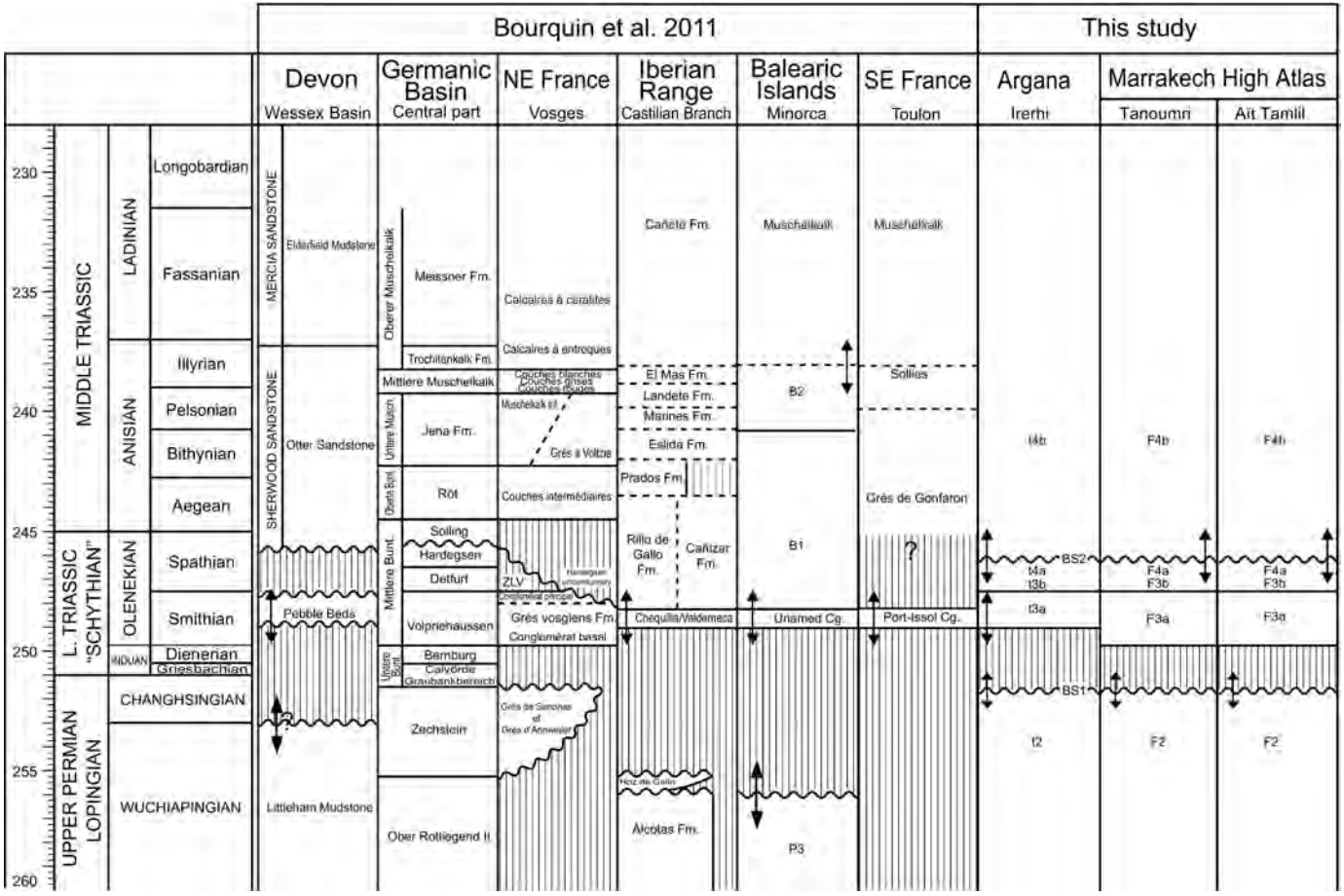
Bourquin et al. 2011
This study
Devon
Wessex Basin
Germanic Basin
Central part
NE France
Vosges
Iberian Range
Castilian Branch
Balearic Islands
Minorca
SE France
Toulon
Argana
Irerhi
Marrakech High Atlas
Tanoumri
Aït Tamlil
MIDDLE TRIASSIC
L. TRIASSIC "SCHYTHIAN"
UPPER PERMIAN LOPINGIAN
LADINIAN
ANISIAN
OLENEKIAN
INDUAN
Longobardian
Fassanian
Illyrian
Pelsonian
Bithynian
Aegean
Spathian
Smithian
Dienerian
Griesbachian
CHANGHSINGIAN
WUCHIAPINGIAN
230
235
240
245
250
255
260
MERCIA SANDSTONE
SHERWOOD SANDSTONE
Elderfield Mudstone
Otter Sandstone
Pebble Beds
Littleham Mudstone
Oberer Muschelkalk
Meissner Fm.
Trochitenkalk Fm.
Mittlere Muschelkalk
Unterer Muschelkalk
Jena Fm.
Oberer Buntsandstein
Röt
Mittlerer Buntsandstein
Solling
Hardegsen
Detfurt
Volpriehaussen
Unterer Buntsandstein
Bernburg
Calvörde
Graubankbereich
Zechstein
Ober Rotliegend II
Calcaires à cératites
Calcaires à entroques
Couches blanches
Couches grises
Couches rouges
Muschelkalk inf.
Grès à Voltzia
Couches intermédiaires
ZLV
Conglomérat principal
Grès vosgiens Fm.
Conglomérat basal
Grès de Sarrolles et Grès d'Annweiler
Cañete Fm.
El Mas Fm.
Landete Fm.
Marines Fm.
Eslida Fm.
Prados Fm.
Rillo de Gallo Fm.
Cañizar Fm.
Chequilla/Valdemeca
Alcolea Fm.
Muschelkalk
B2
B1
Unamed Cg.
P3
Sollies
Grès de Gonfaron
Port-Issol Cg.
t4b
t4a
t3b
t3a
t2
BS2
BS1
F4b
F4a
F3b
F3a
F2

Figure 12